1   **Graphical abstract**
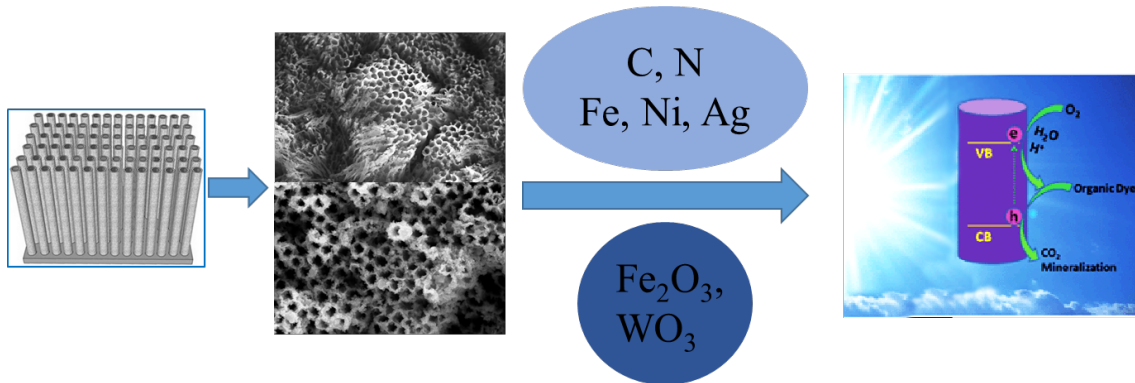
2   Graphic abstract mainly focuses on the preparation and modification of

3   photocatalytic degradation of organic pollutants by anodized TiO_2

4   nanotubes. The TiO_2 nanotubes have higher photocatalytic activity under

5   visible light after heat treatment or water-assisted treatment, and then

6   modification methods such as doping and surface modification.

7

1 **Recent progress in anodic oxidation of TiO₂ nanotubes and enhanced**

2 **photocatalytic performance: a short review**

3 Xiaojiang Nie [1, 2], Siqi Yin [1, 2], Wenchao Duan [1, 2], Zilong Zhao[3], Liang Li[4],

4 Zhiqiang Zhang [1, 2, *]

5 [1] Key Lab of Electromagnetic Processing of Materials, Ministry of Education,

6 Northeastern University, Shenyang, 110819, PR China; [2] College of Materials Science

7 and Engineering, Northeastern University, Shenyang, 110819, PR China; [3] School of

8 Mechanical Engineering and Automation, Fuzhou University, Fuzhou, 350116, PR

9 China; [4] Department of Engineering, School of Engineering and Computer Science,

10 University of Hertfordshire, Hatfield, AL109AB, UK

11

12 *Corresponding author.

13 E-mail address: zqzhang@mail.neu.edu.cn (Z. Zhang).

1 **Recent progress in anodic oxidation of TiO$_2$ nanotubes and enhanced**

2 **photocatalytic performance: a short review**

3 **ABSRTACT**

4 By adjusting the oxidation voltage, electrolyte, anodizing time and other

5 parameters, TiO$_2$ nanotubes with high aspect ratio can be prepared by oxidation

6 in organic system because anodic oxidation method has the advantage of simple

7 preparation process, low material cost and controllable morphology. Low

8 material cost and controllable morphology by anodizing. This review focuses on

9 the influence of anodizing parameters on the morphology of TiO$_2$ nanotube

10 arrays prepared by anodizing. In order to improve the photocatalytic activity of

11 TiO$_2$ nanotubes under visible light and prolong the life of photo-generated

12 carriers, the research status of improving the photocatalytic activity of TiO$_2$

13 nanotubes in recent years is reviewed. This review focuses on the preparation and

14 modification of TiO$_2$ nanotubes by anodic oxidation, which is helpful to

15 understand the best structure of TiO$_2$ nanotubes and the appropriate modification

16 methods, thus guiding the application of TiO$_2$ nanotubes in practical

17 photocatalysis. Finally, the development of TiO$_2$ nanotubes is prospected.

20 **1 Introduction**

21 TiO$_2$ is nontoxic, acid and alkali resistant, high in chemical stability and excellent in

22 biological phase. Since Fujishima and Honda first reported light-induced water splitting

23 on the surface of TiO$_2$ in 1972,[1] it has been widely used in photocatalysis, dye-

24 sensitized cells, biomedicine and other fields. The TiO$_2$ is easy to generate electron-hole

25 pairs when it is excited by external energy. Therefore, most of the organic pollutants

26 could be degraded into CO$_2$ and H$_2$O without secondary pollution. Thus, TiO$_2$ has

27 become a common catalyst for treating organic pollutants. P25, a commonly used

28 photocatalyst in the market at present, has high photocatalytic activity, but TiO$_2$ powder

1   and photocatalytic activity are difficult to recover and further improve, respectively.

2   Due to quantum size effect and surface effect of nano-materials, nano-TiO_2 exhibits

3   better performance than conventional TiO_2.

4   One-dimensional TiO_2 nanotube array is easy to separate photo-generated carriers

5   due to its special morphology, such as large aspect ratio and specific surface area,[2]

6   which has become a promising photochemical/photoelectrochemical material.[3-5]

7   Therefore, TiO_2 nanotubes are widely used in photocatalytic degradation.[6, 7] TiO_2 is a

8   wide band gap N-type semiconductor ($\geq$3.0 eV), the electron-hole pair can be generated

9   only after TiO_2 absorbs photons with wavelength less than 387.5 nm. TiO_2 has high

10   photocatalytic activity only under ultraviolet light, so the utilization rate of solar energy

11   will be reduced, and only about 7 % of the solar spectrum will be absorbed. In addition,

12   photo-generated carriers generated by TiO_2 excitation are easy to recombine, which

13   limits the application of TiO_2 nano-photocatalyst.

14   **2 Factors Affecting Structure and Morphology of TiO_2 Nanotubes by**
15   **Anodizing**

16   There are various methods for preparing One-dimensional TiO_2 nanotubes, such as sol-

17   gel method,[8, 9] template-assisted method,[10, 11] hydrothermal/solvothermal method,[12, 13]

18   and electrochemical method.[14, 15] Since Zwilling et al.[16] initially reported the

19   preparation of TiO_2 nanotube arrays, the preparation of TiO_2 nanotubes by anodic

20   oxidation has become a hot research topic among researchers in recent years. The

21   experimental principle setting is shown in Fig. 1a.[17] Moreover, the dense oxides or TiO_2

22   nanotubes can be formed according to different electrolytes (Fig. 1b). The diameter and

23   length of the nanotubes can be controlled by different parameters through the anodic

24   oxidation method, which provides a better solution for controlling the morphology of

25   nanotubes. In general, the diameter of TiO_2 nanotubes prepared by anodic oxidation

1 (tens of nanometers to hundreds of nanometers) is larger than that of TiO_2 nanotubes

2 prepared by hydrothermal method (more than ten nanometers). Therefore, it is

3 necessary to adjust various process parameters to prepare nanotubes with high aspect

4 ratio and preferable regularity and uniformity.
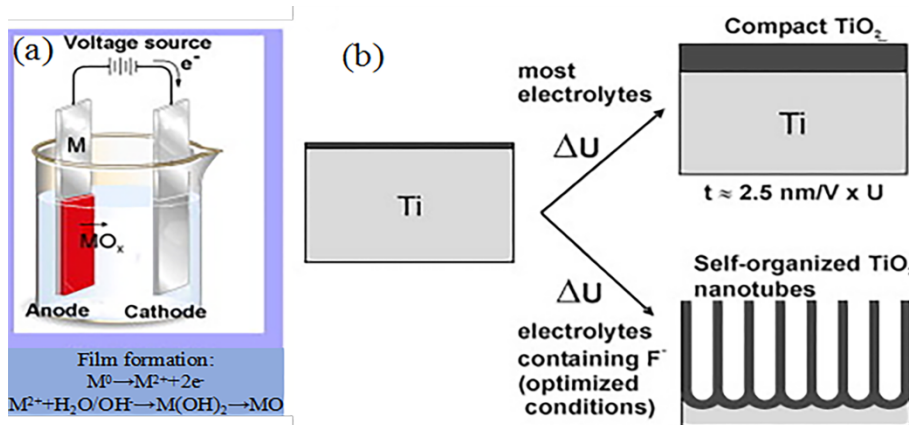
5

6 **Fig. 1** (a) Schematic device of anodic oxidation experiment. (b) Anodic oxidation leads to oxidation

7 of metal substances, forming solid oxides on the metal surface.[17]

8   At present, there are various controversies about the formation mechanism of TiO_2

9 nanotube arrays. Nonetheless, the formation mechanism of this ordered nanotube array

10 structure has not been perfectly explained. The generally accepted mechanisms of

11 porous structure formation are field-assisted dissolution theory and field-assisted

12 injection theory.[18] The theory of "field dissolution" was first applied to explain the

13 formation mechanism of anodic oxide film on aluminium surface.[19] The typical current-

14 time (j-t) curve is plotted and demonstrated in Fig. 2. The whole oxidation process

15 consists of three stages: the initial oxidation film formation, porous oxide film

16 formation, and nanotube arrays formation and stable growth. Firstly, when the voltage is

17 applied, Ti^{4+} and O^{2-} are produce by dissolution and water, respectively. Meanwhile,

18 the electricity separation near the anode forms a dense TiO_2 initial oxidation film, the

19 loop current decreases exponentially.[20] After the initial oxide film is formed, O^{2-} near

1   the anode passes through the oxide film and reaches the interface between the oxide

2   film and titanium substrate under the action of electric field force, which leads to realize

3   field oxidation growth. On the other hand, F^- in the electrolyte combines with Ti^{4+} in the

4   TiO_2 film to generate TiF_6^{2-}. In addition, TiF_6^{2-} is also produced by chemically attack of

5   the formed TiO_2($TiO_2+4H^++6F^-=[TiF_6]^{2-}+2H_2O$), which leads to realize field-induced

6   dissolution.[21] Stress and crystallization in the film layer lead to uneven energy

7   distribution and F^- distribution, resulting in uneven oxide film surface, pore nucleus

8   formation and subsequent pore formation. The un-oxidized Ti matrix bulge at the

9   bottom of the small hole enhances the electric field, accelerates the dissolution of the

10   top oxide film, and turns the small hole into a small cavity.[22] The current gradually

11   increases with the field-induced oxidation increases. At the end, the small cavities

12   gradually deepen to form continuous and independent nanotube arrays. With the

13   extension of oxidation time, the nanotube array grows stably and the current tends to be

14   stable when the growth rate and dissolution rate reach equilibrium.[23] According to the

15   theory of "field dissolution", porous anodic oxide are formed at metal/oxide interface,

16   while dissolution occurs at the electrolyte/oxide interface. However, the reason of the

17   metal ions migrated from metal/oxide interface to electrolyte/oxide interface before the

18   formation of oxide can't be explained. To solve this problem, the field-assisted injection

19   theory was developed. Under the condition of high current efficiency, oxide grows on

20   two interfaces, while under the condition of relatively low current efficiency, metal ions

21   moving outward are directly injected into electrolyte at electrolyte/oxide interface.[24]
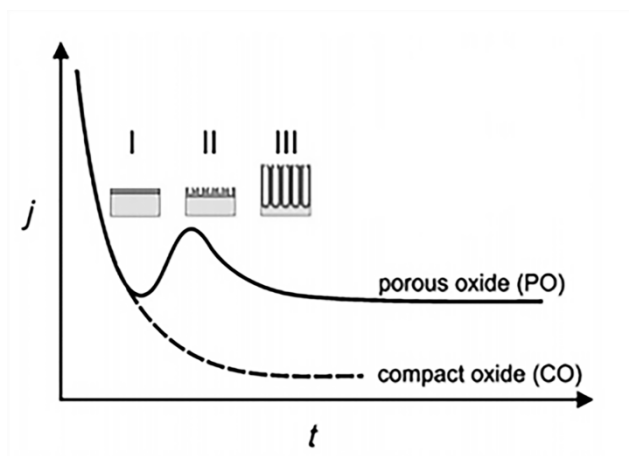
1

2 **Fig. 2** Typical current-time (j-t) characteristics after voltage step in the absence of (---) and the

3 presence of (—) fluoride ions in the electrolyte. Dense oxides (fluoride-free) or porous/tubular metal

4 oxides (fluoride-containing) are formed through different morphological stages (I–III).[18]

5   The theory of "field dissolution" explains the formation of holes and the deepening

6 of channels, but it can't explain the formation mechanism of gaps between nanotubes.[25]

7 At the same time, TiO_2 nanotube arrays can also be obtained in fluorine-free electrolyte

8 system,[26, 27] which proves that the "field dissolution" effect of fluorine ions in the

9 growth process of nanotubes is controversial. Moreover, as we know, F^- participates in

10 the field-assisted dissolution or ejected reaction to reduce current efficiency and volume

11 expansion coefficient. However, the total volume of nanotubes is basically the same

12 under the given current condition, which has nothing to do with the concentration of F^-

13 .[28, 29] Based on the field dissolution theory, the growth of nanotubes is stable. The

14 reason is that the oxide formation rate at the metal/oxide interface is equal to the

15 dissolution rate at the electrolyte/oxide interface, but this balance has not been verified.

16 On the contrary, there is evidence to prove that this balance does not exist.[30, 31]

17 Therefore, in recent years, the field-assisted dissolution theory has been widely

18 challenged.[32-34]

19   The theory of "field dissolution" holds that nanotubes are formed in a "top-down"

20 excavation mode, while the tracer atomic method proves that the formation of

1   nanotubes is opposite.[35] Based on this result, a new theory "viscous flow and stress

2   model theory" is proposed,[36] which holds that under the stress caused by electrostriction

3   or volume expansion stress, the barrier oxide fluid grows from bottom to top along the

4   pipe wall under high electric field, and finally forms the nanotube array structure.[24]

5   Moreover, viscous flow caused by the existence of internal stress in oxide during

6   nanotube growth has been proved.[37] Fig. 3 simultaneously shows stress and current

7   density measurements during the continuous anodizing experiment at 20 V.[38] In the first

8   stage, the initial barrier oxide grows and produces compressive stress at the constant

9   rate of 0.4 minutes. In the second stage, the compressive force is further increased, and

10 then the tensile stress is continued for 20 minutes the oxide is separated and nanotubes

11 are formed at this stage. In the third stage, the stress increases in the compression

12 direction and the thickness of the nanotube layer increases in the remaining time of the

13 anodizing cycle.[25]
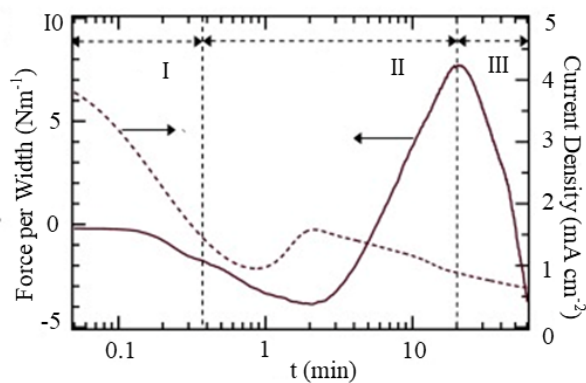
14

15 **Fig. 3** Stress and current density transients at 20 V in 0.1 M NH_4F and 1.6 wt % water in ethylene

16 glycol.[38]

17   However, the viscous flow model can't explain how the nanotube embryo is

18 formed, nor can it explicitly indicate whether the barrier oxide grows at two interfaces

19 or one interface at the bottom of the nanotube.

1   Based on the viscous flow model and avalanche breakdown theory,[37, 39] an oxygen

2   bubble model and a double current model are proposed to explain the relationship

3   between the nanotube morphology and current density-time curve. Double current

4   model refers to ion current and electron current model. The ratio of the two currents can

5   be controlled by adjusting the concentration of NH_4F.[40] Zhu et al put forward the kinetic

6   model of porous anodic oxide,[41] in which ion current was used to form oxide, and

7   electron current was caused by impurity center in oxide, which was used to generate

8   oxygen or spark. For a given electrolyte, electron current depends on impurity center

9   and is independent of ion current. The formation of nanopores can be attributed to the

10   precipitation of oxygen in oxides. Oxygen starts to release at the critical thickness, that

11   is, oxide growth keeps the channel wall lengthening and oxygen evolution keeps the

12   channel unblocking. By controlling the release rate of oxygen under different pressures,

13   the shape of the channel can be adjusted.[41] Regular and uniform thin films can be

14   obtained with the stable current density.[42] Electron current and oxygen release have a

15   key influence on the formation of porous layer.[43] Oxygen bubble model theory can

16   explain the experimental phenomenon that contradicts the field-assisted dissolution

17   theory and has been recognized by many researchers.[44, 45] Especially for some special

18   nanostructures formed by anodic oxidation, the oxygen bubble model has a well

19   explanation.[46, 47] The cavity between the double walls of nanotubes obtained by anodic

20   oxidation in electrolyte containing NH_4F and H_3PO_4 provides direct evidence of pore

21   formation caused by oxygen bubbles.[48] Under this model, the formation diagram of

22   nanotubes is shown in Fig. 4. In the stage I, a dense layer is formed under the front layer.

23   In stage II–IV, the oxides exposed to electrolyte are usually contaminated by anions

24   (usually fluorine). Once anions are introduced into the contaminated layer, they will

25   soon meet the growth layer to form nanotube embryos. In stage II, the contaminated

layer does not reach the grown oxide. At this stage, O_2 bubbles are generated and trapped between the contaminated layer and the preformed layer. With the pollution in stage III, the accumulated O_2 may break the pre-layer, thus forming small cracks on the pre-layer. When the pollution reaches the growth layer, the nanotube embryo begins to grow in stage IV. In stage V, oxygen bubbles destroy the oxide layer and the electrolyte enters the nanotube. Oxide and nanotube grow steadily.[49]
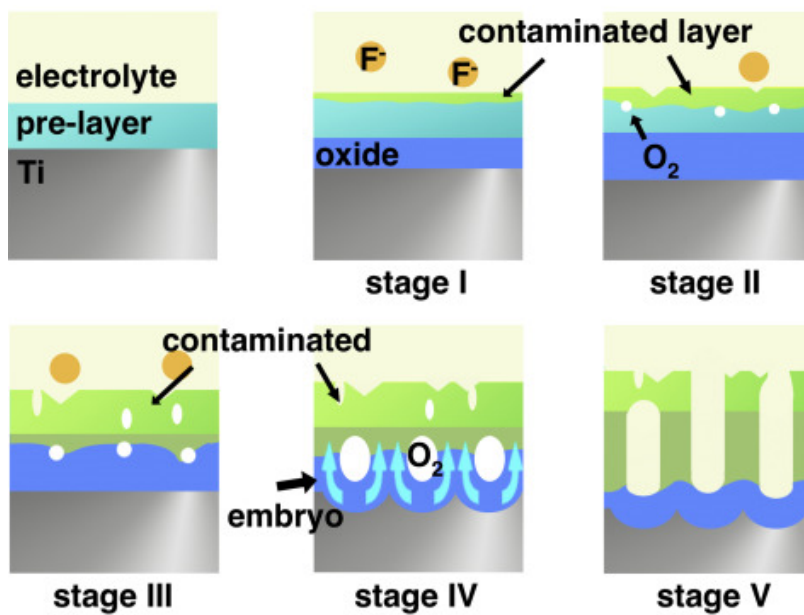
Fig. 4 The mechanism diagram of TiO_2 embryo initiation.[49]

Fig, 5 shows the typical current-time curves of three stages (I, II and III respectively). Under the condition of constant voltage anodic oxidation, the initial high electric field intensity produces relatively high ion current, which decreases with the increase of oxide thickness, as shown in stage I. With the increase of the thickness of barrier layer and the accumulation of anions near the oxide surface, the electron current increases exponentially when the barrier layer grows to the critical thickness and the electric field intensity drops to the critical value. Due to the sufficient electron current, the release of oxygen remains in the anion contaminated layer. Closed small bubbles appear as bubble mold, which leads to the formation of pore embryo in stage II. With

1 the growth of barrier oxide, oxygen bubbles grow and expand upward. Until the oxygen

2 bubble breaks, the electrolyte is allowed to enter, and the total anodic oxidation current

3 reaches quasi-steady state (the stage III).[50] The larger electron current leads to the rapid

4 overflow of oxygen bubbles on the anode membrane surface, while the barrier oxide

5 produced by the small ion current cannot surround the oxygen bubbles, and only a dense

6 membrane can be obtained. The balance between the ion current and electron current

7 can lead to the formation of nanotubes.[51]
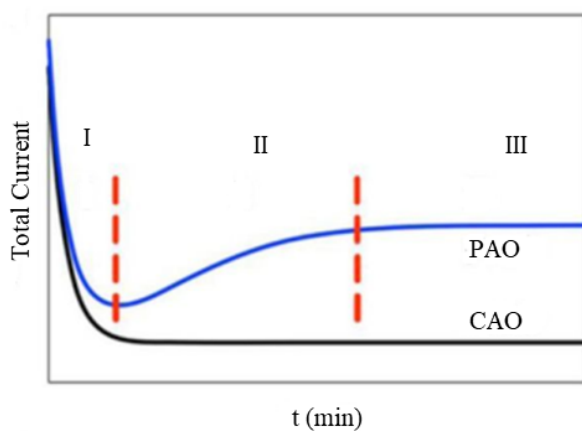
8

9 **Fig. 5** The current-time curve of porous anodic oxide(PAO) or compact anodic

10 oxide(CAO) prepared by constant voltage anodic oxidation.[52]

11   In fact, because the formation mechanism is hard to be derived by direct in-situ

12 experiments, it is difficult to successfully explain the formation mechanism of

13 nanotubes by a single theoretical model, but well results can be obtained by combining

14 various theories.[53] If the plastic flow model is combined with the oxygen bubble model,

15 the formation of gaps and ribs around the anode TiO_2 nanotubes can be successfully

16 clarified.[54] Based on the oxygen bubble model and oxide flow model, the formation

17 mechanism of lotus-root-like nanostructures is proposed.[55]

18 *2.1 Surface pre-treatment*

19 Nowadays, there are extensive researches on the influence of anodic oxidation

1 parameters on the morphology of TiO₂ nanotubes,[28, 56] but few researches are focused

2 on the influence of anodic pre-treatment on the morphology of TiO₂ nanotubes. Cold-

3 working Ti plate produces an intermediate structure between self-organized nanotubular

4 and nanoporous morphology(Fig. 6a). The thickness decreases with the increase of

5 cold-working amount. Long-time thermal annealing after cold-working can eliminate

6 the defects of cold-working and form good nanotube morphology.[57] The residual stress

7 in Ti foil can be eliminated by heat treatment of Ti plate, which is beneficial to reduce

8 the diameter of anodized TiO₂ nanotube array and obtain good morphology with

9 uniform arrangement. With the increase of annealing temperature, the growth rate of

10 TiO₂ nanotubes increases.[58] Surface roughness of Ti can induce higher growth rate

11 (extended nanotube length) and improved self-organization.[59] So that the grinding or

12 polishing Ti plate affects the morphology of anodized TiO₂ nanotubes. Surface

13 irregularities caused by grinding make it easier to form nanonuclei, but their growth is

14 more disordered. Therefore, unlike the smooth surface formed by polishing, the

15 distribution of surface nanotubes on the ground surface is sparser and the height is more

16 irregular. The polished surface forms nanotubes with larger outer diameter and wall

17 thickness(Fig. 6b, c).[60] Different polishing methods (chemical polishing and mechanical

18 polishing) also affect the TiO₂ nanotubes formed by subsequent anodic oxidation.[61]

19
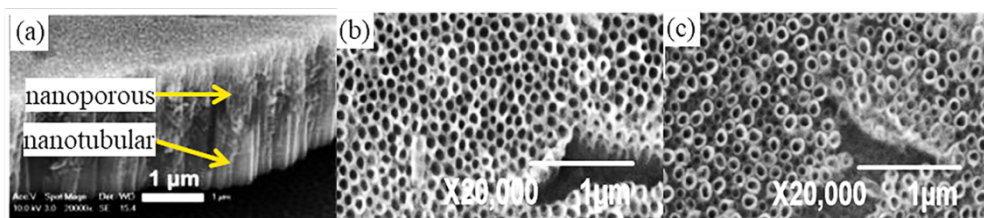
20 **Fig. 6** (a) Intermediate structure of nanotubes and nanopores,[57] and SEM images of the

21 anodized surfaces (b) ground and (c) polished.[60]

1   *2.2 Oxidation Voltage*

2   The research shows that the anodic oxidation voltage has a great influence on the

3   formation of the tube.[62, 63] Low voltage easily forms a mixed structure both at the top

4   nanopore layer and the bottom nanotube layer.[64] High voltage leads to rapid dissolution

5   of TiO_2, attenuation or fracture of the formed nanotubes, and even breakdown of Ti

6   plate.[65] Therefore, TiO_2 nanotube arrays can only be oxidized within a certain voltage

7   range, which is called "voltage window". Mor et al. found that the voltage window was

8   10-23 V when anodizing Ti plates in HF solution system.[66] For organic electrolyte, the

9   voltage window is generally higher than that of aqueous electrolyte.[67] In addition, the

10   oxidation voltage is also related to the diameter and length of nanotubes.[68] The

11   structural characteristics of anodized TiO_2 nanotubes, such as grain size, inner pore size

12   and outer pore size, increase with the increasing anodizing voltage.[69, 70] As the oxidation

13   voltage increases, the diameter and length of nanotubes increase, and the linearity

14   depends on the oxidation voltage.[71] Furthermore, the voltage also affects the tube

15   spacing and tube morphology of TiO_2 nanotubes. Within the limited voltage range from

16   10 V to 40 V, the self-organized spacing of TiO_2 nanotubes can be obtained from 21

17   nm~168 nm,[72] and the tube length gradually increases with the increase of voltage(Fig.

18   7a, b, c).[73] However, when the applied potential exceeds a critical value (usually higher

19   than 60 V), the diameter of the porous anodized nanostructure decreases(Fig. 7d), and

20   the critical value is determined by the electrolyte,[74, 75] therefore, the aspect ratio is

21   reduced. While decreasing the voltage can reduce the porosity and increase the

22   roughness coefficient and aspect ratio of TiO_2 nanotubes. At the same time, decreasing

23   the voltage can separate TiO_2 nanotubes prepared by anodic oxidation in the second-

24   step from the titanium substrate, and obtain independent TiO_2 nanotubes with closed

25   end and hexagonal structure.[76] If square voltage is applied to Ti sheet, the morphology

1   and morphological characteristics of the nanotubes will be changed, and bamboo-knot

2   walls will be formed.[77]
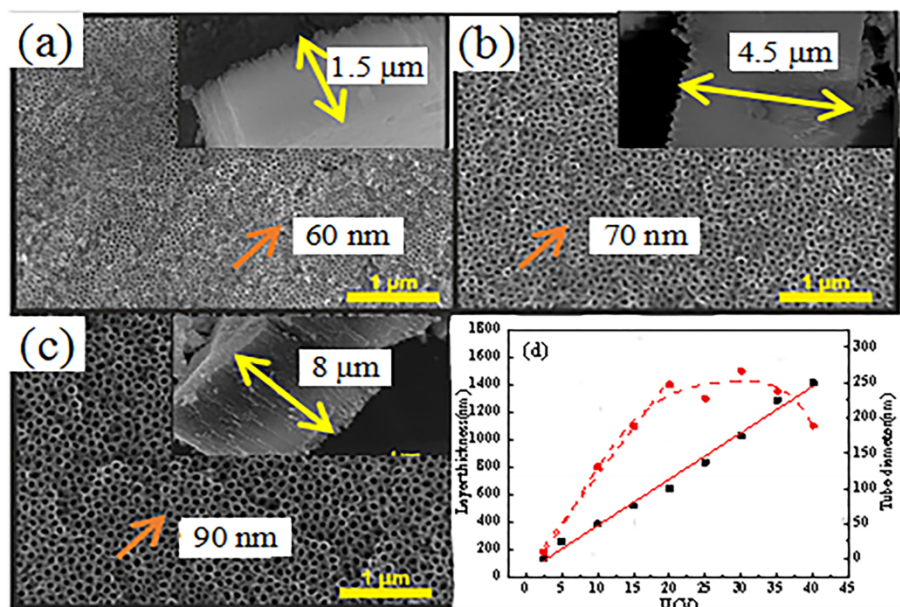
4   **Fig. 7** The morphology of surface and cross section of TiO_2 nanotubes obtained at (a) 20 V, (b) 30 V,

5   (c) 40 V for 60 minutes respectively in the solution system of NH_4F/ethylene glycol,[73] and (d)

6   variation curve of inner diameter and length of TiO_2 nanotubes with voltage.[75]

7   *2.3 Electrolyte*

8   After continuous development, anodizing electrolytes have experienced four

9   generations of electrolyte types: the first generation is HF-containing aqueous

10   electrolytes,[78] the second generation is buffered neutral aqueous electrolytes with

11   fluoride salts (such as KF, NaF),[79] the third generation is viscous organic electrolytes

12   containing fluoride (such as NH_4F/ethylene glycol),[80] and the fourth generation is non-

13   fluoride-based electrolytes (such as HCl).[81]

14   Ethylene glycol containing NH_4F and H_2O is widely used because it can produce

15   nanotubes with uniform diameter and smooth walls.[82] The pH value, F^- concentration

16   and water content in the electrolyte affect the formation and dissolution of oxide film.

14

1   Temperature mainly affects the migration rate of ions in electrolyte. Therefore,

2   temperature is very important for the formation of TiO_2 nanotubes.[83] Anodizing is

3   usually carried out at room temperature, because it is beneficial to the formation of TiO_2

4   nanotubes in this temperature range. However, by changing the electrolyte temperature,

5   it is found that TiO_2 nanotubes can be formed in a large temperature range. In this

6   temperature range, there is no significant change in the diameter of nanotubes, but the

7   wall thickness of TiO_2 nanotubes changes significantly.[4] At low temperature, the rate of

8   oxide dissolution reaction is slower than that of titanium etching, resulting in the

9   formation of thicker nanotube walls.[84] At high temperature, the rate of chemical etching

10   is faster than that of anodic oxidation, and no nanotube structure is formed at this time.[85]

11   Elevated temperature accelerates the formation of TiO_2 nanotubes, and at the same time,

12   it also aggravates the chemical corrosion on the top, so it is unfavourable to prepare

13   longer TiO_2 nanotubes. However, if only the Ti surface is heated and the electrolyte is

14   kept at a low temperature, the TiO_2 nanotubes can grow rapidly and a high aspect ratio

15   can be obtained.[86] The hydrolysis content increases with the increasing pH value,

16   resulting in a large amount of hydrated TiO_2 deposited on the surface of nanotubes.[87]

17   Shorter and cleaner nanotubes are formed with lower pH value, while higher pH value

18   could cause longer nanotubes to suffer unnecessary precipitation. Alkaline solution is

19   not conducive to the formation of self-organized nanotubes.[88] F^- is mainly related to the

20   dissolution of oxide film. The nanotube length increases to the maximum value and then

21   gradually decreases with the increase of NH_4F concentration. If the concentration is

22   very high, the nanotubes become disordered and irregularly arranged, forming a very

23   thick precipitate on the TiO_2 film.[89] Typical F^- concentration is between 0.3 wt% and

24   0.5 wt%.[90, 91]

1   When the electrolyte contains no water or its content is low, the diffusion of H^+

2 and F^- ions in high viscosity ethylene glycol electrolyte is inhibited. With the increase of

3 water content, the concentration of H^+ increases gradually, the electrochemical

4 oxidation rate is faster than the chemical dissolution rate, and the tube length of TiO_2

5 nanotubes increases. However, when excessive water is added, the H^+ concentration

6 increases to the point where the chemical dissolution rate is higher than the

7 electrochemical oxidation rate, which leads to the destruction of the oriented tubular

8 structure, and even completely dissolves to form nanoparticles.[92] In addition, the

9 solution viscosity of NH_4F and ethylene glycol electrolyte is very unfavourable to the

10 diffusion of various ions in the electrolyte, so the uniformity of electrolyte also has a

11 great influence on the morphology of TiO_2 nanotubes. The morphology of TiO_2

12 nanotubes can be better than that of prepared without stirring before anodic oxidation or

13 during oxidation.[93, 94] The increase of stirring rate has little effect on the morphology of

14 TiO_2 nanotubes, but the higher the stirring rate, the more serious the fracture of TiO_2

15 nanotubes.[95] The effects of various electrolyte parameters on the tube diameter, length

16 and wall thickness of anodized TiO_2 nanotubes are shown in Table 1

17 **Table 1** Tube diameter, length and wall thickness of TiO_2 nanotubes prepared with different

18 electrolyte parameters in ethylene glycol system.

Electrolyte parameters	Condition	Tube diameter	Tube length	Wall thickness	References
Water content	2 wt%	52.73 nm	21.8 μm	36.91 nm	96
	3 wt%	111.5 nm	25.6 μm	15.75 nm	
	4 wt%	121.2 nm	24.2 μm	31.9 nm	
Temperature	5 °C	Premature pores	No	No	97

	10 °C	35 nm (porous)	No	No	
	25 °C	125 nm	250 nm	30 nm	
	30 °C	175 nm	-	27 nm	
	50 °C	190 nm	-	22 nm	
	70 °C	200 nm	-	20 nm	
NH$_4$F content	0.1 wt%	45.1 nm	4.479 μm	94.1 nm	
	0.3 wt%	50.2 nm	4.243 μm	65.75 nm	28
	0.5 wt%	49.4 nm	4.421 μm	47.2 nm	
	No	60 nm	0.66 μm	6.7 nm	
Stirrer rate	150 rpm	62 nm	0.75 μm	13.3 nm	95
	300 rpm	62 nm	0.71 μm	6.7 nm	
	600 rpm	61 nm	0.67 μm	6.7 nm	

1   - means that this data is not available in the references

2   *2.4 Anodizing steps*

3   The multiple oxidation of TiO$_2$ is to form ordered hexagonal depressions on the Ti

4   substrate through the first anodic oxidation, which serves as a template for the further

5   growth of TiO$_2$ nanotubes. The first anodic oxidation is actually the surface pre-

6   treatment of Ti foil and the first anodic oxidation could provide ordered marks. TiO$_2$

7   nanotube arrays with more uniform diameter and arrangement order can be obtained by

8   multiple anodic oxidation methods.[98] However, due to the active nature of the Ti

9   substrate, an excessively thick oxide film may form before the sunken substrate reacts

10   again. Thus, multiple anodization may deteriorate the morphology of nanotubes.

1   TiO$_2$ nanotubes grown in the second step of anodization are obviously superior to

2   TiO$_2$ nanotubes prepared by conventional one-step Ti anodization in terms of size

3   uniformity and arrangement order. By adjusting the experimental parameters in the

4   second step of anodization, two new types of TiO$_2$ nanostructures are obtained: lotus

5   root-like nanostructures, double-layer nanotube arrays with bamboo-like upper part and

6   smooth wall lower part.[99] The TiO$_2$ nanotube array constructed by the third anodization

7   shows more regular structure than the sample constructed by the conventional single

8   anodization.[100] In addition, as anodic oxidation moves from the first, second and third

9   steps, the diameter of the inner pores of TiO$_2$ nanotubes increases, but the wall thickness

10   of TiO$_2$ nanotubes gradually decreases.[101] By carefully studying the influence of

11   multiple anodizing on the morphology and geometric properties of TiO$_2$ nanotubes, it is

12   found that the length of TiO$_2$ nanotubes increased sharply by two-step anodizing, which

13   is from 2 μm in one-step anodizing to 4 μm in two-step anodizing. In addition, it also

14   has high roughness factor, surface area and aspect ratio, as well as very orderly structure

15   and clear opening (Fig. 8).[102, 103]
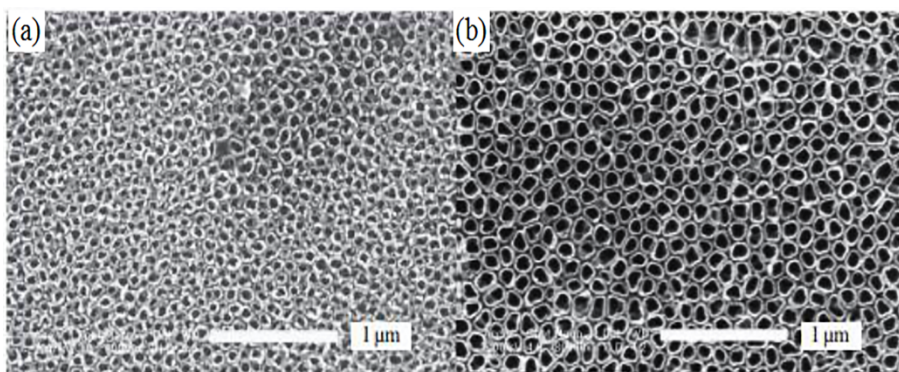
16

17   **Fig. 8** SEM images of TiO$_2$ nanotubes under different anodizing steps (a) one-step

18   oxidation and (b) two-step oxidation.[103]

19   *2.5 Oxidation Time*

20   When the TiO$_2$ porous oxide film is formed, the tube length of TiO$_2$ nanotubes

1   gradually increases with the increasing oxidation time. In addition, with the further

2   extension of oxidation time, the diameter of TiO_2 nanotubes increases similarly.[104] For

3   NH_4F solution organic system, as the solution has a certain viscosity, ion transport is

4   slow and oxidation time is long (usually as long as several hours).[105, 106] If the oxidation

5   time is short, only TiO_2 porous oxide film can be formed without TiO_2 array.[107] With

6   the increase of anodizing time, the diameter of nanotubes may increase linearly (Fig. 9a,

7   b, c, d),[108] or increases and decreases repeatedly, but eventually increases.[109] However,

8   with the increasing oxide film thickness, the migration rate of H^+ and F^- plasma

9   decreases, the increase of tube length gradually slows down, and finally reaches

10   stability(Fig. 9e).[110]
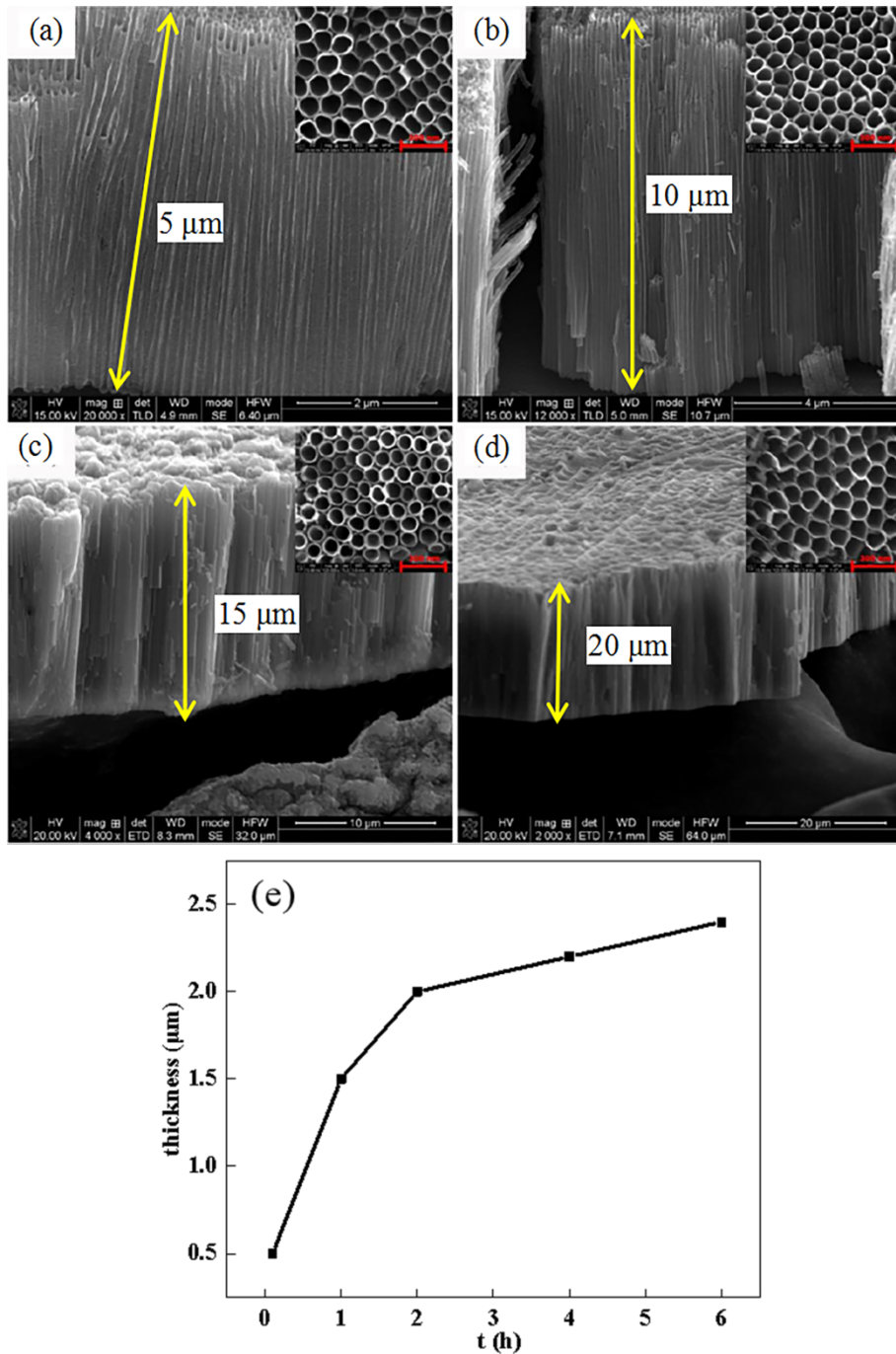
Fig. 9 Surface morphology of TiO_2 nanotubes under different oxidation time (a) 1 h, (b) 3 h, (c) 5 h, (d) 7 h [108] and (e) wall thickness of TiO_2 nanotubes under different oxidation time.[110]

2.6 In-situ radiation

In recent years, in-situ radiation has been used to adjust the structure of TiO_2 nanotubes. For example, when the TiO_2 nanotubes are prepared by anodic oxidation under ultraviolet-visible(UV-vis) radiation, because of the photooxidation of water by

1   nanotubes, the concentration of H^+ is higher at the bottom, the nanotubes with larger

2   diameter and thicker wall are produced after irradiation, and the length of nanotubes

3   remains unchanged compared with that without UV-vis radiation.[111] In addition, the

4   thickness of the inner wall and outer wall of the double-walled TiO_2 nanotube prepared

5   with UV assistance can be changed by altering the power of UV light.[112] Aliabadi et al.

6   carefully studied the influence of UV irradiation time on geometric characteristics, and

7   the results showed that the UV irradiation has a significant impact on geometric

8   characteristics in the two-step anodic oxidation process. After irradiation for 120

9   minutes, the size of TiO_2 nanotubes was increased, meanwhile, the surface area,

10   roughness and aspect ratio were also significantly improved.[113]

11   In summary, the structure of TiO_2 nanotubes is affected by oxidation voltage,

12   electrolyte, oxidation times and other parameters. The three stages of the oxidation

13   process could be coordinated with each other to obtain TiO_2 nanotubes with desirable

14   structure by adopting appropriate preparation conditions. Albu et al. prepared TiO_2

15   nanotubes with a length of more than 250 μm and a significantly higher aspect ratio in

16   HF acid system for the first time by comprehensively adjusting the voltage, HF acid

17   concentration and oxidation time.[114] The high voltage may break through the Ti plate,

18   which is not conducive to the formation of TiO_2 nanotubes. However, by optimizing the

19   NH_4F content under different voltages, a uniform thin film without any oxide

20   breakdown can be obtained, and ordered TiO_2 nanotubes with high aspect ratio can be

21   rapidly prepared in a few minutes under the high anodic oxidation voltage of 220 V, and

22   the fastest growth rate is 2.45 μm/min.[115]

23   *2.7 Heat treatment and water-assisted treatment*

24   Except for some special cases,[116] TiO_2 nanotubes prepared by anodic oxidation are

amorphous. In order to change them into stable crystalline phase, there are currently two methods: heat treatment and water-assisted treatment. The research shows that the amorphous tube layer is obviously transformed into anatase at about 280 ℃.[117] At about 500 ℃, rutile phase begins to appear. As the temperature further increases, anatase phase disappears and completely transforms into rutile phase.[118] In nanoscale, anatase is relatively stable, while rutile is thermodynamically considered as the most stable bulk phase. However, with the increasing temperature, the morphology of nanotubes will be worse and worse. When Roy annealed nanotubes at 450 ℃, cracks appeared in the tube wall(Fig. 10a).[119] Moreover, with the increasing temperature, the grain size becomes larger, which is the main reason for tube collapse. Tube collapse will significantly affect the specific surface area of TiO_2 nanotubes.

Another method is water-assisted treatment. In 2011, Liao et al. used deionized water to place amorphous TiO_2 nanotubes at room temperature for 3-4 days, and the amorphous nanotubes were transformed into stable anatase phase,[120] and part of TiO_2 nanoparticles would be deposited on the surface and side of nanotubes(Fig. 10b), which significantly increased the specific surface area of TiO_2 nanotubes. The mechanism of water-assisted crystallization is as follows:[121]

$$TiO_{2(a)}+4H_2O \rightarrow Ti(OH)_6^{2-}+2H^+ \tag{1}$$

$$Ti(OH)_6^{2-}+2H^+ \rightarrow TiO_{2(c)}+4H_2O \tag{2}$$
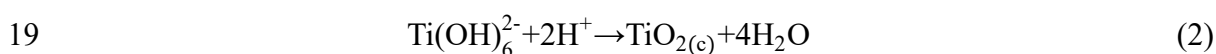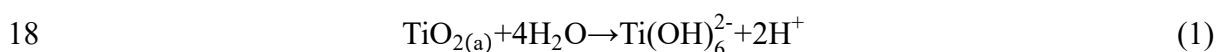
Here, $TiO_{2(a)}$ is amorphous TiO_2 nanotube. $TiO_{2(c)}$ is anatase TiO_2 nanotube.

After that, researches on water-assisted crystallization of TiO_2 nanotubes have emerged one after another.[122-124] The mixed phase of anatase and rutile can be obtained by adding dilute HCl or HNO_3 into deionized water.[125] However, the crystallization cycle of water-assisted TiO_2 nanotubes is longer, and the crystallinity is much lower than that of heat-treated TiO_2 nanotubes. So, for TiO_2 applications requiring higher

1 crystallinity, such as dye-sensitized solar cells, water-assisted TiO_2 nanotube

2 crystallization can't replace heat-treated TiO_2 nanotubes,[126] which also limits the

3 application of water-assisted TiO_2 nanotube crystallization. Therefore, heat treatment is
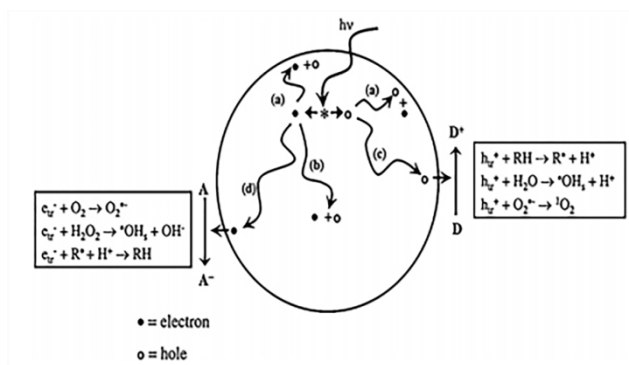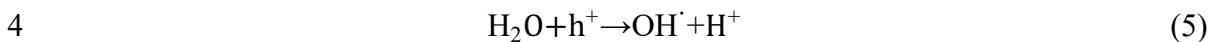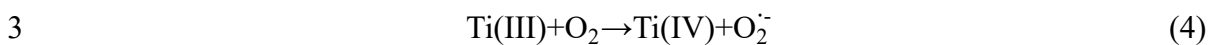
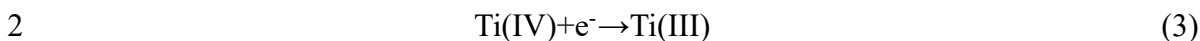4 generally adopted at present.[127, 128]
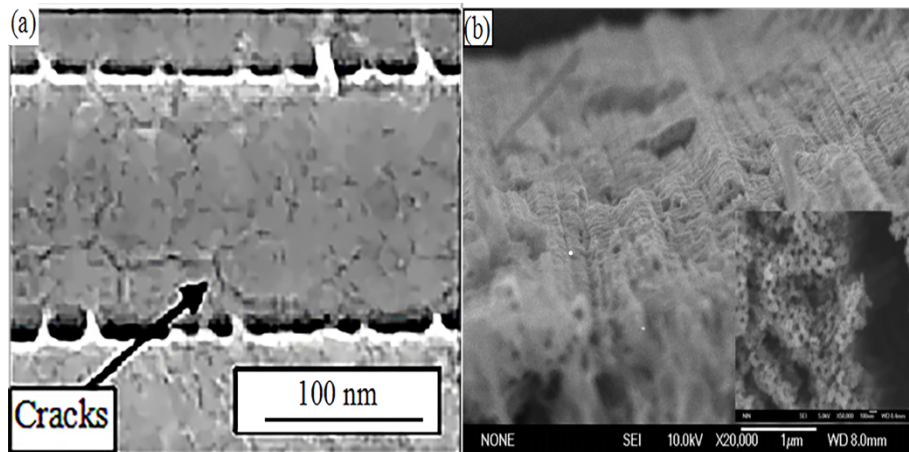
5

6 **Fig. 10** (a) After annealing at 450 ºC, TiO_2 nanotubes with cracks in the tube wall,[119]and (b) Water-

7 assisted treatment of side and surface morphology of TiO_2 nanotubes.[120]

8 **3 Factors Affecting Photocatalytic Activity of TiO_2 Nanotubes**

9 The photocatalytic mechanism of TiO_2 is shown in Fig. 11. After absorption of TiO_2

10 nanoparticles, photons with energy is equal to or higher than their band gap collide, and

11 electrons are excited from the valence band (VB) into the unoccupied conduction band

12 (CB), resulting in excited electrons in the conduction band and positive holes in the

13 valence band. These charge carriers can be recombined nonradiatively or radiatively

14 (dissipating input energy as heat), or captured and reacted with electron donors or

15 receptors adsorbed on the surface of the photocatalyst.[129] At the same time, electrons in

16 the CB usually participate in the reduction process. The reduction process usually reacts

17 with molecular oxygen in air to generate superoxide radical anion (O_2^{2-}), O^{2-} and H^+

18 form H_2O_2, which is further converted into OH^-.[130] These free radicals can oxidize

19 macromolecular pollutants to form non-polluting inorganic small molecules, such as

CO$_2$ and water. The overall mechanism can be summarized as the following steps.[131]

$$Ti(IV)+e^-\rightarrow Ti(III) \tag{3}$$

$$Ti(III)+O_2\rightarrow Ti(IV)+O_2^{\cdot-} \tag{4}$$

$$H_2O+h^+\rightarrow OH^\cdot+H^+ \tag{5}$$

$$OH^\cdot+OP\rightarrow\rightarrow intermediates\rightarrow\rightarrow H_2O+CO_2 \tag{6}$$

$$O_2^{\cdot-}+OP\rightarrow\rightarrow intermediates\rightarrow\rightarrow H_2O+CO_2 \tag{7}$$

Fig. 11 Process occurring on bare TiO$_2$ particles after ultraviolet excitation.[130]

Many researchers have developed photocatalytic fuel systems that can not only degrade organic pollutants in water under visible light, but also make full use of their chemical energy for power generation, thus greatly improving the utilization rate of polluted water (Fig. 12).[132, 133]
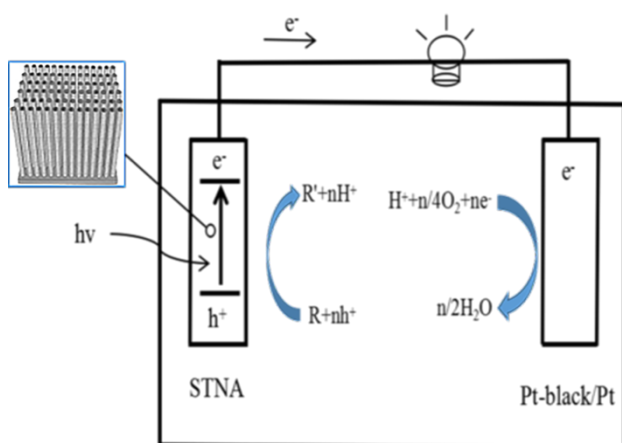
Fig. 12 Schematic diagram of working principle of PFC system based on STNA wherein R and R' are organic compounds and oxidation products thereof.[133]

1   The ideal photocatalyst should exhibit the following characteristics: well chemical

2   corrosion resistance, good light corrosion resistance, ability of absorbing a wide range

3   of UV, vis and even infrared light, and effective charge separation. In addition, the

4   photocatalyst should be made of the elements which are rich in earth, cost-effective,

5   suitable for cheap synthesis methods, and can be used on a large scale.[134] As a common

6   photocatalyst, there are some disadvantages for TiO_2. Firstly, TiO_2 is a semiconductor

7   with a large forbidden band, which has photocatalytic activity only under UV irradiation.

8   Thus, the utilization rate of solar energy is low. Secondly, the photo-generated hole-

9   electron pair excited by TiO_2 is easy to recombine, which will obviously weaken the

10   photocatalytic activity of TiO_2. In order to solve these issues, effective improvement

11   methods include: 1) improving nanotube structure and morphology, 2) introducing other

12   elements, and 3) surface modification.

13   ***3.1 Structure and morphology of TiO$_2$ nanotubes***

14   *3.1.1 Morphology of TiO$_2$ Nanotubes*

15   Compared with these modifications introduced with foreign substances, it is also

16   remarkable to enhance the photocatalytic activity by improving the structure and

17   morphology of TiO_2 nanotubes.[135, 136] As the unique aspect ratio structure of TiO_2

18   nanotubes, it is easy to separate the photo-generated carriers. Thus, the preparation of

19   TiO_2 nanotubes with higher aspect ratio is a way to improve their catalytic

20   performance.[137] With the increasing oxidation voltage and time, the diameter, length

21   and surface area of TiO_2 nanotubes are further increased, and the surface reaction rate

22   constant is linearly related to the surface area.[138] TiO_2 nanotubes grown on Ti substrate

23   are selectively dissolved at the bottom, and then HF acid is used to dissolve the oxide

24   film on the top of the nanotubes. TiO_2 nanotube arrays with open ends are prepared,

which have better permeability and photocatalytic performance.[139, 140] Alternatively, double-walled TiO_2 nanotube arrays can be prepared by imprint technology, and then highly hexagonal ordered single-walled TiO_2 nanotube arrays can be obtained after optimizing chemical treatment in piranha solution, and its catalytic activity is higher than that of classic self-ordered TiO_2 nanotubes.[141] TiO_2 nanotubes with nano grating structure can be prepared by oxidation in fluorine-containing electrolyte, which accelerates electron-hole separation and also provided lower recombination rate.[142] The performance of TiO_2 nanotubes is greatly improved even through simple surface treatment.[143]

The regularity and uniformity of TiO_2 nanotubes and their photocatalytic activity increase with the increasing oxidation voltage. However, if the voltage is excessively high, the regularity will be destroyed and the catalytic activity will be reduced. Therefore, when the oxidation voltage increases to a certain value, the catalytic activity of TiO_2 nanotubes reaches an extreme value (Fig. 13).[144]
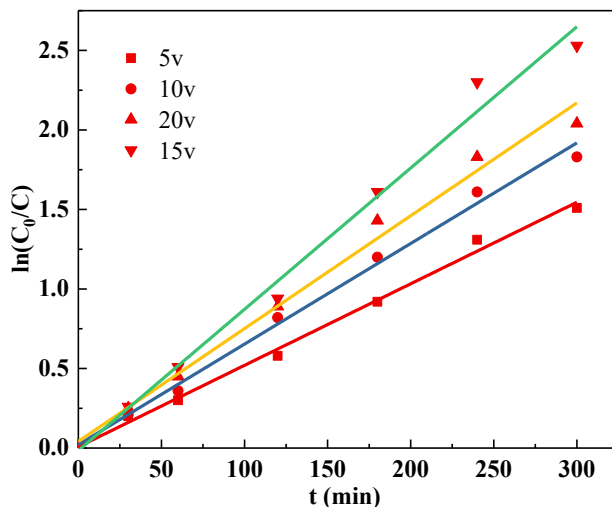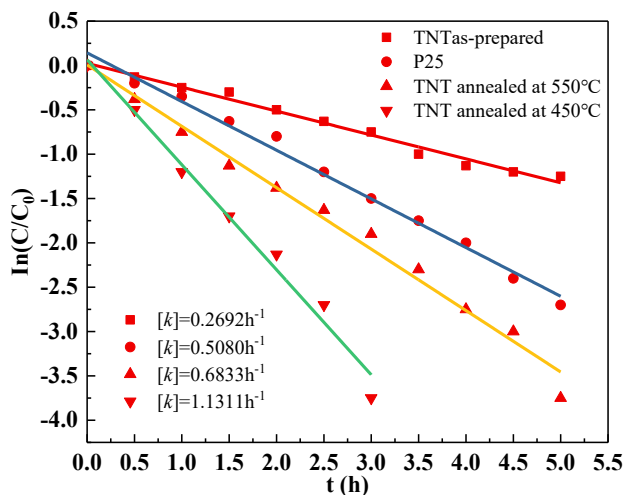

Fig. 13 Photocatalytic activity of TiO_2 nanotubes under different voltages.[144]

3.1.2 Crystalline phase of TiO_2 Nanotubes

Anatase phase is the main photocatalytic phase, and its catalytic activity is better than

26

1   that of amorphous and rutile TiO_2 nanotubes. Early studies have shown that the activity

2   of pure anatase was higher than that of mixed phase.[145, 146] Macak et al.[147] believed that

3   the decrease of anatase is the reason for the decrease in photocatalytic activity (Fig. 14).

4

5   **Fig. 14** Photocatalytic degradation rate of AO7 with different crystal phase structures (▼-anatase

6   phase. ▲-mixed crystal structure of anatase and rutile).[147]

7   However, recent studies have shown that the catalytic activity of the mixed crystal

8   structure of anatase and rutile is higher than that of pure anatase phase.[148, 149] According

9   to the corresponding research, Li et al. showed that when it is annealed at about 500 ℃,

10   anatase and rutile can be obtained in a special layered mixed crystal phase. TiO_2 with

11   mixed crystal structures can effectively inhibit the photogenerated hole-electron

12   recombination, thus having higher catalytic activity.[150] The main photocatalytic phase is

13   the anatase which distributes at the top of the nanotube. However, rutile phase at the

14   bottom of the nanotube may form an internal electric field to promote effective

15   separation of the photo-generated carriers, thus improving the activity. TiO_2 nanotubes

16   prepared in acidic electrolyte can be annealed at 650 ℃ for 30 minutes to obtain a

17   mixed phase of anatase and rutile with the highest crystallinity and also obtain the best

18   catalytic degradation effect on methyl orange.[136]

1   *3.3 Doping Modification*

2   *3.3.1 Non-metallic doping*

3   Non-metallic ion doping modification is a key area in the research of TiO_2 nanotubes,

4   and the doping ions are widely distributed, such as non-metallic cations (I^{5+}, Si^{4+}, etc.),

5   and anions (N, C, etc.). However, the B ion is special, which can replace Ti^{4+} in the

6   crystal lattice in the form of B^{3+}, or replace O^{2-} in the crystal lattice in the form of B^{2-}.[151]

7   Until now, the most successful research is N doping, which can narrow the optical gap

8   and improve the visible light catalytic activity.[152-154] Because N has the atomic size

9   equivalent to oxygen, small ionization energy, formation and stability of metastable

10   center, so it is easier to dope into TiO_2 crystal lattice. Since Asahi et al. successfully

11   doped N in TiO_2 for the first time,[152] the research on the mechanism of enhancing the

12   photocatalytic activity of TiO_2 nanotubes by N doping has become increasingly perfect.

13   [155]After doping, N may also serve as the recombination center of photo-generated

14   carriers, reducing the photocatalytic activity under UV light.[156]The effect of C doping is

15   similar to N doping. It is generally believed that C doping can improve the adsorption of

16   organic molecules and the conductivity of TiO_2.[157] Therefore, C doped TiO_2 nanotubes

17   show better activity than TiO_2 nanotubes under UV light. C doped TiO_2 nanotubes can

18   be prepared by calcining the amorphous TiO_2 nanotubes in air and natural gas

19   atmosphere successively, which reduces the band gap of TiO_2 nanotubes and has higher

20   activity under visible light.[158] However, when the C doping amount is extremely high, C

21   will become the recombination center of electrons and holes, and the catalytic

22   performance will be reduced.[159]

23   Many studies demonstrated that C doping is the substitution of C for O^{2-}, thus

24   forming $TiO_{2-x}C_x$ type C doped TiO_2 nanotubes,[160] while, according to Valentin et al's

25   theory, C was preferred to replace O under anoxic conditions, and was conducive to

1   replace Ti under oxygen-enriched conditions.[161] The diameter of C doped TiO_2

2   nanotubes could be adjusted by changing the flow rate of carrier gas. The optical band

3   gap (2.72 eV) after doping was much smaller than that of anatase TiO_2 (3.20 eV).[162]

4   *3.3.2 Metal doping*

5   The metal doping of TiO_2 nanotubes can be divided into three categories: transition

6   metal ions, rare earth metal ions and noble metal ions. Metal ions are doped into TiO_2

7   lattice to replace Ti^{4+} ions, thus affecting energy band structure and reducing the light

8   absorption edge energy of TiO_2. Karvinen et al. studied the doping effect of various

9   transition metal ions (V^{3+}, Cr^{3+}, Fe^{3+}, etc.) on anatase and rutile, and found that the

10 doping of these ions can obviously reduce the band gap of anatase, but has no effect on

11 the rutile.[163] Rare earth elements have unique 4f orbitals and 5d orbitals, which can

12 reduce the recombination rate of electron-hole pairs. In addition, rare earth elements can

13 effectively prevent grain growth after doping. Compared with other rare earth ions, Gd

14 ion has the smallest energy band gap and grain size after doping, the largest specific

15 surface area and highest photocatalytic activity.[164] Mazierski et al. studied the

16 lanthanide doped TiO_2 nanotubes, and got different conclusions. Under visible light, Ho

17 doped TiO_2 nanotubes had the highest photocatalytic activity, and they thought that the

18 photocatalytic activity under visible light irradiation was not caused by oxygen center,

19 but by other forms of active oxygen ($O_2 \cdot ^-$, $HO_2 \cdot$, H_2O_2).[165] Noble metal deposition is

20 also one of the most effective methods to improve the photocatalytic performance of

21 TiO_2 nanotubes.[165] Noble metals such as (Ag, Au, etc.) can induce charge carriers by

22 light, thus realizing the effective separation of electron-hole pairs and improving the

23 photocatalytic activity.[166, 167] It is generally believed that uniform doping can promote

24 the performance of element-doped TiO_2 nanotubes,[168] while non-uniform doping is

1 detrimental to the performance, because it may lead to partial aggregation of doped

2 elements and become the recombination center of carriers. However, Zhang et al. found

3 that non-uniform doping can form "platinum island" and interface separation effect in

4 Au-doped TiO_2 nanotubes, which is beneficial to isolate photogenerated electrons and

5 holes, so the photocatalytic activity of non-uniform Au-doped TiO_2 is enhanced

6 compared with uniform Au-doped TiO_2 nanotubes.[169] Although metal ions can

7 effectively reduce the band gap of TiO_2, metal ions can easily become the

8 recombination center of electron-hole pairs, which will reduce the photocatalytic

9 activity.[170]

10 *3.3.3 Co-doping of Multiple Elements*

11 Although the doping of single element makes the photocatalytic performance of TiO_2

12 nanotubes better than that of un-doped TiO_2 nanotubes, there is still much room for

13 improvement in photocatalytic activity under visible light. In recent years, many

14 literatures show that the performance of multi-element co-doped TiO_2 nanotubes is

15 obviously higher than that of single-element doped TiO_2 nanotubes due to their

16 synergistic effect.[171, 172]

17   Multi-element co-doping includes metal-metal co-doping, metal-non-metal co-

18 doping, and non-metal-non-metal co-doping. For example, Lanthanum, gallium co-

19 doped TiO_2 nanotubes can accelerate the electron capture and dye adsorption. This is

20 because La^{3+} and Gd^{3+} replace Ti^{4+}, resulting in a large number of oxygen vacancies

21 and surface defects. Thereby accelerating the separation of photo-generated electron-

22 hole pairs and promoting photocatalytic degradation.[173] Co-doping Ti^{3+} and Ni changes

23 the band structure of TiO_2 nanotubes, narrows the band gap to 2.84 eV, and enhances

24 the light absorption. Ni doping widens the VB of TiO_2, which can promote the

separation and transmission process of charge carriers. The performance is about 10 times larger than that of un-doped TiO_2 nanotubes.[174] When metallic element Zr is co-doped with non-metallic element N, and the element ratio of Zr to N is 2:1, the recombination of electron-hole pairs can be effectively inhibited due to the joint action of metal and non-metal, so that TiO_2 nanotubes have higher photocatalytic activity under visible light.[175] Non-metallic element B and metallic element Co are successfully doped into TiO_2 nanotubes for the first time. Because the surface hydroxyl groups have obvious advantages in different current densities, pH values, initial degradation concentrations and degradations of different types of pollutants, the doping of Co significantly enhances the stability of TiO_2 nanotubes, although it is detrimental to photocatalytic activity.[176]

Doping with various of non-metallic elements, such as N and F co-doping, will lead to wormhole-like mesopores, which are beneficial to capture more photons for stimulating the formation of photo-generated carriers, as well as larger surface area and enhanced light absorption, thus having enhanced photocatalytic activity.[177] In addition, the band gap of TiO_2 nanotubes is shortened from 3.2 eV to 3.04 eV by co-doping with three or more non-metallic elements such as C, N, and F. Among all doped non-metallic elements, C, N doping improves the visible light absorption of TiO_2, while F doping leads to the formation of oxygen vacancy. In addition, C doping can also improve the specific surface area of TiO_2 nanotubes, thus having good photocatalytic activity under sunlight.[178]

The general photocatalytic mechanism of doped TiO_2 is shown in Fig. 15. The metal doping produces defect level near the CB of TiO_2, while non-metal doping causes extra defect level above the VB of TiO_2. The defect energy level will shorten the band gap of TiO_2, thus contributing to visible light photoactivity. In co-doped and multi-

31

1   doped TiO_2, electrons can transition from these defect energy levels or the VB of TiO_2

2   to metal defect impurity energy levels, or to the highest energy level of CB of TiO_2.

3   Metal ions in variable oxidation state can be used as electron capture centers. Capture

4   centers lead to the increase of charge carrier life, thus increasing the photocatalytic

5   activity of TiO_2.[179] How to select appropriate co-doping elements to exert synergistic

6   effect and to improve the performance of TiO_2 nanotubes are the theoretical premises of

7   co-doping modification, because the co-doping of some elements will reduce the

8   performance of TiO_2 nanotubes.[180]
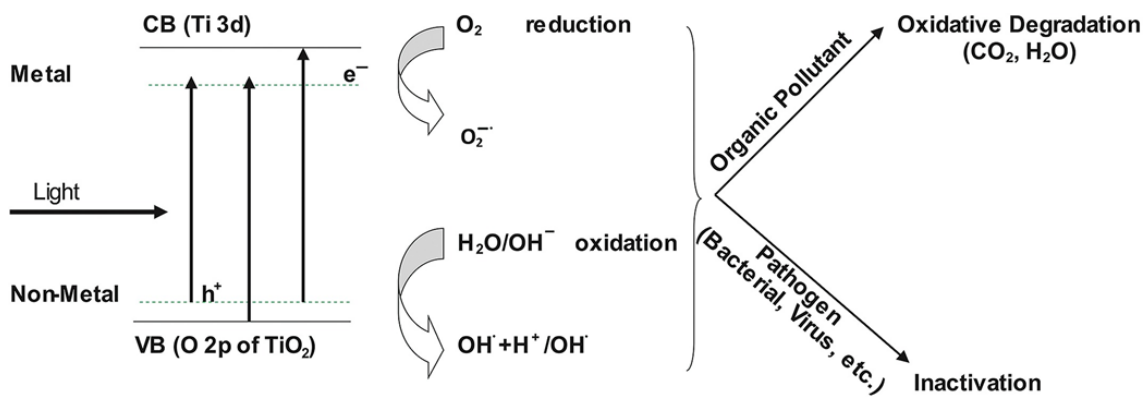
9

10   **Fig. 15** General photocatalytic mechanism of doped TiO_2.[181]

11   *3.4 Filling and Surface Modification*

12   Because photo-generated carriers generated by TiO_2 excitation are easy to recombine,

13   so it is very important to improve the catalytic activity by filling or surface modification

14   to reduce carrier recombination. The recombination of charges e⁻ and h⁺ is reduced,

15   more hydroxyl radicals and peroxides (O^{2-}) are generated, and the photocatalytic

16   degradation of organic matters is promoted.[182]

17   It has been reported that many TiO_2 nanotubes are decorated or filled with different

18   foreign materials.[183-185] In recent years, the photocatalytic activity of TiO_2 nanotubes

19   has been enhanced by constructing heterojunction (more than two layers of different

20   semiconductor thin films are deposited on the same substrate in turn). Fe_2O_3 can form
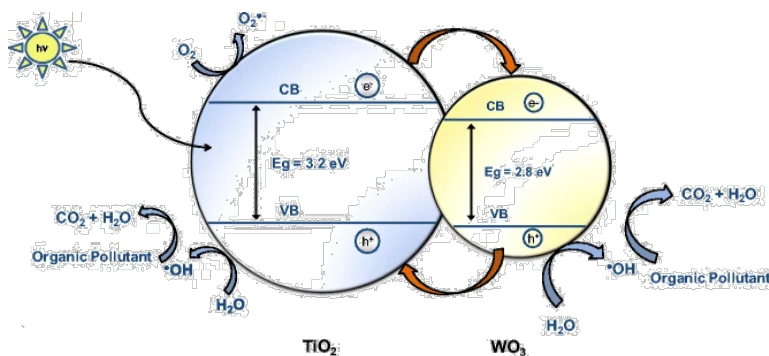
1   the type I heterojunction with TiO_2, which shows enhanced separation of e^-/h^+ pairs and

2   enhanced photocatalytic activity.[186] In addition, similar to co-doping, when multiple

3   materials with synergistic effect sensitize TiO_2 nanotubes, the performance of TiO_2

4   nanotubes is higher than that of single material sensitized TiO_2 nanotubes. However,

5   when materials without synergistic effect are sensitized together, the performance is

6   reduced.[187] Fe_2O_3 and graphite nitrogen carbide ($g-C_3N_4$) are loaded on the surface of

7   N-doped TiO_2 nanotubes, and the excitation energy of TiO_2 nanotubes is reduced due to

8   the loading of N and Fe_2O_3, thus exhibits a lower Eg value (2.15 eV) than single TiO_2

9   nanotubes, N-doped TiO_2 nanotubes and $g-C_3N_4$ loaded N-doped TiO_2 nanotubes. In

10   addition, $g-C_3N_4$ can promote charge migration, so it has higher hydroxyl generation

11   and degradation efficiency (Fig. 16a).[188] This synergistic effect is also applicable to

12   TiO_2 with other structures (Fig. 16b).[189]
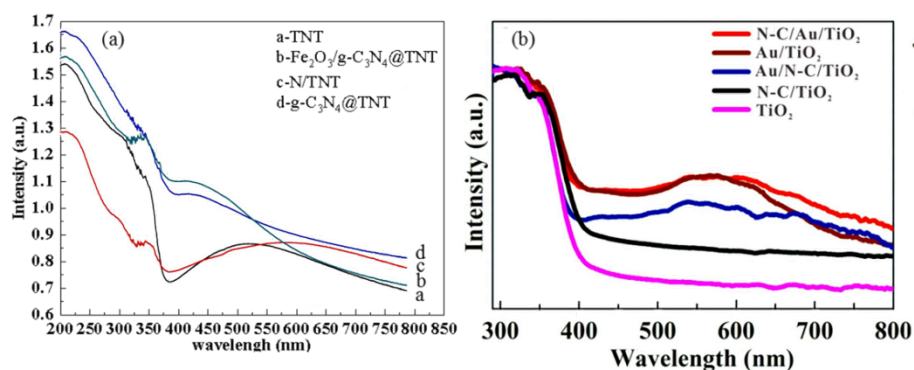
13

14   **Fig. 16** UV-vis diffuse reflectance spectra of different TiO_2 nanotubes[188] and TiO_2 samples.[190]

15   WO_3 has a band position matched with TiO_2, which can form the type II

16   heterojunction (Fig. 17),[191] and the separation of electron-hole pairs is enhanced under

17   visible light.[189] In addition to the WO_3/TiO_2 heterojunction alone, $BiVO_4$ is selected to

18   be introduced into WO_3/ TiO_2 nanotubes, and oxygen vacancy is also introduced. With

19   the introduction of $BiVO_4$, the inherent degradation path dominated by hydroxyl and

20   hole into the degradation path dominated by oxygen vacancy and hole. The stable

21   oxygen vacancy is used to construct the separation and transmission of charge carriers

33

1 in heterogeneous materials, thus realizing the high catalytic performance and stability of

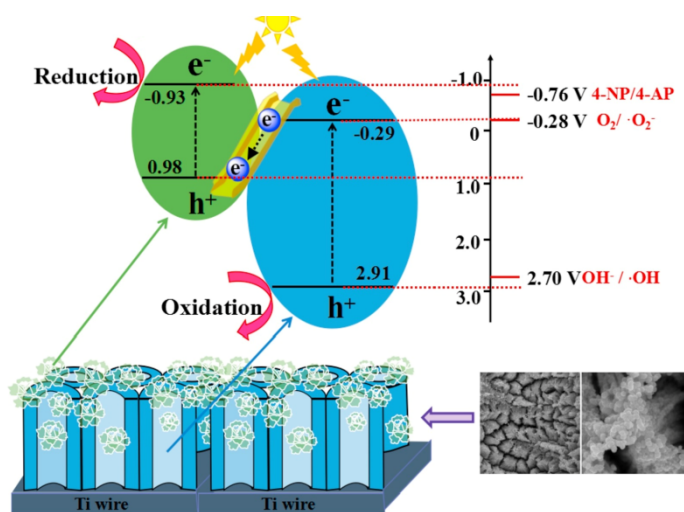2 the composite membrane in degrading volatile organic pollutants.[192]

3

4 **Fig. 17** Mechanisms of degradation proposed for (a) WO_3/TiO_2 and (b) Fe_2O_3/TiO_2.[193]

5   Ag_2O is a visible light active photocatalyst with a band gap of 1.2 eV, which forms

6 a heterojunction with TiO_2 (type III heterojunction). [191]Photogenerated electrons in CB

7 of Ag_2O are transferred into CB of TiO_2, and react with adsorbed O_2 to form O^{2-}. In

8 addition, photogenerated h^+ in VB of Ag_2O reacts with OH^- to form -OH, and

9 participates in degradation.[194]

10   In addition, the Z-scheme structure is another connection mode between the above

11 two semiconductors. Z-scheme structure can reduce the band gap of semiconductor and

12 make CB potential more negative and VB potential more correct. This structure is a

13 promising strategy for improving photocatalysts.[195] Compared with the traditional type

14 II heterostructure, Z-scheme structure can not only realize the effective separation of

15 photogenerated electrons and holes, but also enhances redox ability.[196] By constructing

16 the Z-scheme structure of TiO_2 nanotubes-graphene(GR)-CdS quantum dots, the light

17 absorption range of TiO_2 nanotubes is extended to a wider sunlight area due to the

18 coupling of TiO_2 nanotubes, GR and CdS quantum dots.[197] The principle of

19 photocatalytic degradation of 4-nitrophenol (4-NP) by the direct Z-scheme structure

20 formed by $MoSe_2$ and TiO_2 nanotubes is shown in Fig. 18, the electrons (-0.93 V)

21 stored in the CB of $MoSe_2$ are mainly captured by 4-NP ions and reduced to form 4-

aminophenol. Furthermore, the absorbed water molecules are easily oxidized to free radicals . OH by the holes (2.91V) accumulated in high potential TiO_2 VB. Then, the benzene ring of 4-NP is easily attacked by free radical . OH and degraded into small organic molecules. In addition, highly ordered anodic TiO_2 nanotubes are beneficial to the reaction of transferred free radicals . OH with adsorbed organic molecules, thus realizing the effective removal of 4-NP.[198]

Fig. 18 Mechanism of photocatalytic degradation of 4-NP by $MoSe_2@TiO_2$ nanotubes direct Z-Scheme composite under sunlight.[198]

Of course, there are still other types of heterojunctions. By constructing the 0D/1D heterostructure of GdS quantum dots/TiO_2 nanotubes, the combination of CdS quantum dots and TiO_2 nanotubes significantly accelerates the process of trapping electrons in the heterostructure. Furthermore, the recombination lifetime of electrons at the shallow and deep traps with holes can be extended to 73.2 ps and 622.6 ps, respectively.[199]

4 Conclusions

In this paper, the preparation and modification of anodized TiO_2 nanotubes in recent years are briefly reviewed. Due to the novel physical properties of vertically aligned TiO_2 nanotubes prepared by anodic oxidation, anodic oxidation method is widely used. However, there are still many problems to be solved, including the lack of clear

35

explanation of many basic mechanisms and the development of TiO_2 nanotubes with significant photocatalytic activity under sunlight. In recent years, the rapid development in the preparation and modification of anodized TiO_2 nanotubes has enabled TiO_2 nanotubes to meet the increasingly severe challenges of photocatalysts, so as to cope with the practical application of environmental pollution. However, the inherent wide band gap of TiO_2 nanotubes is the main bottleneck which restricts its wide applications. In order to improve the visible light photocatalytic activity of TiO_2 nanotubes, various means are needed to change the electronic structure and energy band structure of the crystal, or to reduce the recombination rate of electron-hole pairs. Some new modification methods developed in recent years make the practical application of TiO_2 nanotubes longer. Facing the increasingly serious environmental pollution problem, the photocatalyst- TiO_2 nanotube is playing an important role in protecting our environment.

Acknowledgements

Conflicts of interest

There is no conflict of interest.

References

1. H. K. Fujishima A. *Nature.* **238**, 37 (1972).
2. K. Shankar, G. K. Mor, H. E. Prakasam, S. Yoriya, M. Paulose, O. K. Varghese, C. A. Grimes. *Nanotechnology.* **18**, (2007).
3. K. Shankar, J. I. Basham, N. K. Allam, O. K. Varghese, G. K. Mor, X. J. Feng, M. Paulose, J. A. Seabold, K. S. Choi, C. A. Grimes. *Journal of Physical Chemistry C.* **113**, 6327 (2009).
4. G. K. Mor, K. Shankar, M. Paulose, O. K. Varghese, C. A. Grimes. *Nano Lett.* **5**, 191 (2005).
5. Y. Zhao, N. Hoivik, K. Y. Wang. *Nano Energy.* **30**, 728 (2016).
6. P. Mazierski, J. Luczak, W. Lisowski, M. J. Winiarski, T. Klimczuk, A. Zaleska-Medynska. *Appl Catal B-Environ.* **214**, 100 (2017).
7. J. S. Souza, W. A. Alves. *J. Nanosci. Nanotechnol.* **20**, 5390 (2020).
8. Y. L. Pang, S. Bhatia, A. Z. Abdullah. *Sep Purif Technol.* **77**, 331 (2011).

9. T. Kasuga, M. Hiramatsu, A. Hoson, T. Sekino, K. Niihara. *Langmuir.* **14**, 3160 (1998).

10. M. Karaman, F. Sariipek, O. Koysuren, H. B. Yildiz. *Applied Surface Science.* **283**, 993 (2013).

11. H. J. Shin, D. K. Jeong, J. G. Lee, M. M. Sung, J. Y. Kim. *Adv Mater.* **16**, 1197 (2004).

12. B. Abida, L. Chirchi, S. Baranton, T. W. Napporn, C. Morais, J. M. Leger, A. Ghorbel. *Journal of Power Sources.* **241**, 429 (2013).

13. S. D. Perera, R. G. Mariano, K. Vu, N. Nour, O. Seitz, Y. Chabal, K. J. Balkus. *Acs Catal.* **2**, 949 (2012).

14. J. G. Yu, B. Wang. *Appl Catal B-Environ.* **94**, 295 (2010).

15. D. Kuang, J. Brillet, P. Chen, M. Takata, S. Uchida, H. Miura, K. Sumioka, S. M. Zakeeruddin, M. Gratzel. *Acs Nano.* **2**, 1113 (2008).

16. V. Zwilling, E. Darque-Ceretti, A. Boutry-Forveille, D. David, M. Y. Perrin, M. Aucouturier. *Surf Interface Anal.* **27**, 629 (1999).

17. J. M. Macak, H. Tsuchiya, A. Ghicov, K. Yasuda, R. Hahn, S. Bauer, P. Schmuki. *Curr Opin Solid St M.* **11**, 3 (2007).

18. P. Roy, S. Berger, P. Schmuki. *Angew Chem Int Ed Engl.* **50**, 2904 (2011).

19. T. P. Hoar, N. F. Mott. *Journal of Physics and Chemistry of Solids.* **9**, 97 (1959).

20. D. Regonini, C. R. Bowen, A. Jaroenworaluck, R. Stevens. *Mat Sci Eng R.* **74**, 377 (2013).

21. J. V. Pasikhani, N. Gilani, A. E. Pirbazari. *Mater Res Express.* **5**, (2018).

22. J. L. Zhao, X. H. Wang, R. Z. Chen, L. T. Li. *Solid State Commun.* **134**, 705 (2005).

23. K. Indira, U. K. Mudali, T. Nishimura, N. Rajendran. *Journal of Bio- and Tribo-Corrosion.* **1**, (2015).

24. D. J. LeClere, A. Velota, P. Skeldon, G. E. Thompson, S. Berger, J. Kunze, P. Schmuki, H. Habazaki, S. Nagata. *J Electrochem Soc.* **155**, C487 (2008).

25. Q. Dou, P. Shrotriya, W. F. Li, K. R. Hebert. *Electrochim Acta.* **295**, 418 (2019).

26. C. L. Chang, X. B. Huang, Y. P. Liu, L. Bai, X. N. Yang, R. Q. Hang, B. Tang, P. K. Chu. *Electrochim Acta.* **173**, 345 (2015).

27. F. Hu, X. Lin, S. L. Zhu, X. J. Yang, Z. D. Cui. *Applied Surface Science.* **258**, 3260 (2012).

28. Z. Y. Zhang, Q. Wang, H. Q. Xu, W. C. Zhang, Q. Y. Zhou, H. P. Zeng, J. L. Yang, J. W. Zhu, X. F. Zhu. *Electrochemistry Communications.* **114**, (2020).

29. Z. Y. Zhang, Q. Q. Liu, M. F. He, F. R. Tang, Z. R. Ying, H. Q. Xu, Y. Song, J. W. Zhu, X. F. Zhu. *J Electrochem Soc.* **167**, (2020).

30. M. S. Yu, H. M. Cui, F. P. Ai, L. F. Jiang, J. S. Kong, X. F. Zhu. *Electrochemistry Communications.* **86**, 80 (2018).

31. J. J. Zhang, W. Q. Huang, K. Zhang, D. Z. Li, H. Q. Xu, X. F. Zhu. *Electrochemistry Communications.* **100**, 48 (2019).

32. K. Zhang, S. K. Cao, C. Li, J. R. Qi, L. F. Jiang, J. J. Zhang, X. F. Zhu. *Electrochemistry Communications.* **103**, 88 (2019).

33. Q. Zhou, D. Niu, X. Feng, A. Wang, X. Zhu. *Electrochemistry Communications.* **119**, 106815 (2020).

34. M. S. Yu, Y. Chen, C. Li, S. Yan, H. M. Cui, X. F. Zhu, J. S. Kong. *Electrochemistry Communications.* **87**, 76 (2018).

35. S. J. Garcia-Vergara, P. Skeldon, G. E. Thompson, H. Habazaki. *Electrochim Acta.* **52**, 681 (2006).

36. W. Lee, S. J. Park. *Chem Rev.* **114**, 7487 (2014).

37. O. O. Capraz, P. Shrotriya, P. Skeldon, G. E. Thompson, K. R. Hebert. *Electrochim Acta.* **167**, 404 (2015).

38. Q. Dou, P. Shrotriya, W. F. Li, K. R. Hebert. *Electrochim Acta.* **292**, 676 (2018).

39. Y. Li, Z. Y. Ling, X. Hu, Y. S. Liu, Y. Chang. *Rsc Adv.* **2**, 5164 (2012).

40. M. S. Yu, W. K. Zhang, S. Y. Zhang, S. W. Zhao, F. P. Ai, X. F. Zhu. *Surf Coat Tech.* **334**, 500 (2018).

41. X. F. Zhu, Y. Song, L. Liu, C. Y. Wang, J. Zheng, H. B. Jia, X. L. Wang. *Nanotechnology.* **20**, (2009).

42. D. Xu, X. Feng, Y. Song, X. Li, X. Shen. *Electrochemistry Communications.* 106822 (2020).

43. H. Y. Lu, H. W. Fan, R. Jin, B. Chong, X. P. Shen, S. Yan, X. F. Zhu. *Electrochim Acta.* **215**, 380 (2016).

44. W. Q. Huang, H. Q. Xu, Z. R. Ying, Y. X. Dan, Q. Y. Zhou, J. J. Zhang, X. F. Zhu. *Electrochemistry Communications.* **106**, (2019).

45. S. Y. Zhang, D. H. Yu, D. D. Li, Y. Song, J. F. Che, S. Y. You, X. F. Zhua. *J Electrochem Soc.* **161**, E135 (2014).

46. X. F. Zhu, L. Liu, Y. Song, H. B. Jia, H. D. Yu, X. M. Xiao, X. L. Yang. *Monatsh Chem.* **139**, 999 (2008).

47. D. D. Li, L. A. Zhao, C. H. Jiang, J. G. Lu. *Nano Lett.* **10**, 2766 (2010).

48. M. S. Yu, C. Li, Y. B. Yang, S. K. Xu, K. Zhang, H. M. Cui, X. F. Zhu. *Electrochemistry Communications.* **90**, 34 (2018).

49. S. W. Zhao, C. Li, T. F. Wei, C. Y. Li, M. S. Yu, H. M. Cui, X. F. Zhu. *Electrochemistry Communications.* **91**, 60 (2018).

50. B. Chong, D. L. Yu, R. Jin, Y. Wang, D. D. Li, Y. Song, M. Q. Gao, X. F. Zhu. *Nanotechnology.* **26**, (2015).

51. Q. Y. Zhou, M. M. Tian, Z. R. Ying, Y. X. Dan, F. R. Tang, J. P. Zhang, J. W. Zhu, X. F. Zhu. *Electrochemistry Communications.* **111**, (2020).

52. S. W. Zhao, J. Xing, H. W. Fan, S. Y. Zhang, D. D. Li, X. F. Zhu. *J Electrochem Soc.* **164**, E187 (2017).

53. X. F. Zhu, Y. Song, D. L. Yu, C. S. Zhang, W. Yao. *Electrochemistry Communications.* **29**, 71 (2013).

54. B. Chong, D. L. Yu, M. Q. Gao, H. W. Fan, C. Y. Yang, W. H. Ma, S. Y. Zhang, X. F. Zhu. *J Electrochem Soc.* **162**, H244 (2015).

55. R. Jin, H. W. Fan, Y. T. Liu, W. Ma, H. Y. Lu, P. Yang, W. H. Ma. *Electrochim Acta.* **188**, 421 (2016).

56. I. P. Torres-Avila, I. I. Padilla-Martinez, N. Perez-Hernandez, A. E. Banuelos-Hernandez, J. C. Velazquez, J. L. Castrejon-Flores, E. Hernandez-Sanchez. *Coatings.* **10**, (2020).

57. H. Li, L. X. Zheng, S. W. Shu, H. Cheng, Y. Y. Li. *J Electrochem Soc.* **158**, C346 (2011).

58. W. He, S. J. Park, D. H. Shin, S. J. Yoon, Y. Wu, J. Qiu, Y. H. Hwang, H. K. Kim, B. Kim. *J Korean Phys Soc.* **58**, 575 (2011).

59. A. Apolinario, C. T. Sousa, J. Ventura, J. D. Costa, D. C. Leitao, J. M. Moreira, J. B. Sousa, L. Andrade, A. M. Mendes, J. P. Araujo. *J Mater Chem A.* **2**, 9067 (2014).

60. V. Jordanovova, M. Losertova, M. Stencek, T. Lukasova, G. S. Martynkova, P. Peikertova. *Materials.* **13**, (2020).

61. H. Budiman, R. Wibowo, O. Zuas, J. Gunlazuardi, Iop, Photo-electrochemical properties of TiO_2 nanotube arrays: effect of different polishing method of Ti substrate prior to anodization in fluoride-H_2O_2-containing electrolyte. In *9th International*

Conference on Physics and Its Applications, Iop Publishing Ltd: Bristol, 2019; Vol. 1153.

62. S. P. Albu, P. Schmuki. *Electrochim Acta.* **91**, 90 (2013).

63. K. Lee, A. Mazare, P. Schmuki. *Chem Rev.* **114**, 9385 (2014).

64. Y. Sun, K. P. Yan. *Int J Hydrogen Energ.* **39**, 11368 (2014).

65. C. C. Chen, J. H. Chen, C. G. Chao, W. C. Say. *J Mater Sci.* **40**, 4053 (2005).

66. G. K. Mor, O. K. Varghese, M. Paulose, N. Mukherjee, C. A. Grimes. *J Mater Res.* **18**, 2588 (2003).

67. S. K. Mohapatra, M. Misra, V. K. Mahajan, K. S. Raja. *J Catal.* **246**, 362 (2007).

68. I. M. Mehedi, M. F. Hossain, T. Takahashi, M. S. Islam. *J Photoch Photobio A.* **335**, 200 (2017).

69. J. Kapusta-Kolodziej, K. Syrek, A. Pawlik, M. Jarosz, O. Tynkevych, G. D. Sulka. *Applied Surface Science.* **396**, 1119 (2017).

70. M. M. Muzakir, Z. Zainal, H. N. Lim, A. H. Abdullah, N. N. Bahrudin, M. S. M. Ali. *Energies.* **13**, (2020).

71. S. Bauer, S. Kleber, P. Schmuki. *Electrochemistry Communications.* **8**, 1321 (2006).

72. S. Ozkan, N. T. Nguyen, A. Mazare, I. Cerri, P. Schmuki. *Electrochemistry Communications.* **69**, 76 (2016).

73. J. Gomes, J. Lincho, E. Domingues, M. Gmurek, P. Mazierski, A. Zaleska-Medynska, T. Klimczuk, R. M. Quinta-Ferreira, R. C. Martins. *Sci Total Environ.* **689**, 79 (2019).

74. Z. Su, M. Buhl, W. Zhou. *J Am Chem Soc.* **131**, 8697 (2009).

75. J. M. Macak, H. Hildebrand, U. Marten-Jahns, P. Schmuki. *J Electroanal Chem.* **621**, 254 (2008).

76. Javad, Vahabzadeh, Pasikhani, Neda, Gilani, Azadeh, Ebrahimian, Pirbazari. *Nano-Structures & Nano-Objects.* (2016).

77. H. P. Quiroz, J. E. Serrano, A. Dussan. *J. Alloy. Compd.* **825**, 8 (2020).

78. D. Gong, C. A. Grimes, O. K. Varghese, W. C. Hu, R. S. Singh, Z. Chen, E. C. Dickey. *J Mater Res.* **16**, 3331 (2001).

79. A. Ghicov, H. Tsuchiya, J. M. Macak, P. Schmuki. *Electrochemistry Communications.* **7**, 505 (2005).

80. S. Ozkan, F. Valle, A. Mazare, I. Hwang, N. Taccardi, R. Zazpe, J. M. Macak, I. Cerri, P. Schmuki. *Acs Appl Nano Mater.* **3**, 4157 (2020).

81. N. K. Allam, K. Shankar, C. A. Grimes. *J Mater Chem.* **18**, 2341 (2008).

82. J. M. Macak, H. Tsuchiya, L. Taveira, S. Aldabergerova, P. Schmuki. *Angewandte Chemie-International Edition.* **44**, 7463 (2005).

83. T. Ghani, M. Mujahid, M. Mehmood, M. Ubaidullah, A. Shah, A. Mahmood. *J Electron Mater.* **49**, 1881 (2020).

84. H. C. Liang, X. Z. Li. *J. Hazard. Mater.* **162**, 1415 (2009).

85. M. Erol, T. Dikici, M. Toparli, E. Celik. *J. Alloy. Compd.* **604**, 66 (2014).

86. V. Asgari, M. Noormohammadi, A. Ramazani, M. A. Kashi. *J Porous Mat.* (2020).

87. G. K. Mor, O. K. Varghese, M. Paulose, K. Shankar, C. A. Grimes. *Sol Energ Mat Sol C.* **90**, 2011 (2006).

88. Q. Y. Cai, M. Paulose, O. K. Varghese, C. A. Grimes. *J Mater Res.* **20**, 230 (2005).

89. Y.-C. Lim, Z. Zainal, M. Z. Hussein, W.-T. Tan, Morphology and Dimensions Controlled of Titania Nanotubes in Mixed Organic-Inorganic Electrolyte. In *Green Technologies for Sustainable & Innovation in Materials*, Harun, M. K.; Yahya, M. Z. A.; Abdullah, S.; Chan, C. H., Eds. 2013; Vol. 686, pp 13.

90. A. Kaczmarek, T. Klekiel, E. Krasicka-Cydzik. *Surface and Interface Analysis.* **42**, 510 (2010).

91. C. C. Chen, S. J. Hsieh. *J Electrochem Soc.* **157**, K125 (2010).

92. Y. Sun, Q. Zhao, G. X. Wang, K. P. Yan. *J. Alloy. Compd.* **711**, 514 (2017).

93. H. F. Li, M. Ding, J. Jin, D. Sun, S. Zhang, C. K. Jia, L. D. Sun. *Chemelectrochem.* **5**, 1006 (2018).

94. Y. J. Chang, J. W. Lee, H. P. Chen, L. S. Liu, G. J. Weng. *Thin Solid Films.* **519**, 3334 (2011).

95. R. Liu, W. D. Yang, L. S. Qiang, J. F. Wu. *Thin Solid Films.* **519**, 6459 (2011).

96. Z. Jedi-Soltanabadi, M. Ghoranneviss, Z. Ghorannevis, H. Akbari. *Vacuum.* **155**, 387 (2018).

97. L. Mohan, C. Dennis, N. Padmapriya, C. Anandan, N. Rajendran. *Mater Today Commun.* **23**, (2020).

98. Z. B. Yang, D. Y. Pan, C. Xi, J. H. Li, J. W. Shi, F. Xu, Z. Q. Ma. *Journal of Power Sources.* **236**, 10 (2013).

99. S. Q. Li, G. M. Zhang, D. Z. Guo, L. G. Yu, W. Zhang. *Journal of Physical Chemistry C.* **113**, 12759 (2009).

100. J. J. Gong, Y. K. Lai, C. J. Lin. *Electrochim Acta.* **55**, 4776 (2010).

101. S. C. Han, J. M. Doh, J. K. Yoon, G. H. Kim, J. Y. Byun, S. H. Han, K. T. Hong, S. I. Kwun. *Met Mater Int.* **15**, 493 (2009).

102. J. V. Pasikhani, N. Gilani, A. E. Pirbazari. *Solid State Sci.* **84**, 57 (2018).

103. Z. X. Peng, J. H. Ni. *Roy Soc Open Sci.* **6**, (2019).

104. S. Palmas, A. Da Pozzo, F. Delogu, M. Mascia, A. Vacca, G. Guisbiers. *Journal of Power Sources.* **204**, 265 (2012).

105. H. Wang, H. Y. Li, J. S. Wang, J. S. Wu. *Mater Lett.* **80**, 99 (2012).

106. O. K. Varghese, D. W. Gong, M. Paulose, C. A. Grimes, E. C. Dickey. *J Mater Res.* **18**, 156 (2003).

107. V. A. Sugiawati, F. Vacandio, A. Galeyeva, A. P. Kurbatov, T. Djenizian. *Front Phys-Lausanne.* **7**, (2019).

108. Z. Yi, Y. Zeng, H. Wu, X. F. Chen, Y. X. Fan, H. Yang, Y. J. Tang, Y. G. Yi, J. Q. Wang, P. H. Wu. *Results Phys.* **15**, (2019).

109. S. Y. Yoo, H. G. Park. *Korean J Met Mater.* **57**, 521 (2019).

110. J. M. Macak, K. Sirotna, P. Schmuki. *Electrochim Acta.* **50**, 3679 (2005).

111. Y. R. Smith, B. Sarma, S. K. Mohanty, M. Misra. *ACS Appl. Mater. Interfaces.* **4**, 5883 (2012).

112. G. Ali, H. J. Kim, J. J. Kim, S. O. Cho. *Nanoscale.* **6**, 3632 (2014).

113. B. G. Aliabadi, N. Gilani, J. V. Pasikhani, A. E. Pirbazari. *Ceram. Int.* **46**, 19942 (2020).

114. S. P. Albu, A. Ghicov, J. M. Macak, R. Hahn, P. Schmuki. *Nano Lett.* **7**, 1286 (2007).

115. Z. Chamanzadeh, M. Noormohammadi, M. Zahedifar. *Mater Res Express.* **5**, (2018).

116. L. Giorgi, T. Dikonimos, R. Giorgi, F. Buonocore, G. Faggio, G. Messina, N. Lisi. *Nanotechnology.* **29**, (2018).

117. H. Y. Hwang, A. A. Prabu, D. Y. Kim, K. J. Kim. *Sol Energy.* **85**, 1551 (2011).

118. A. Ghicov, S. P. Albu, R. Hahn, D. Kim, T. Stergiopoulos, J. Kunze, C. A. Schiller, P. Falaras, P. Schmuki. *Chem Asian J.* **4**, 520 (2009).

119. P. Roy, D. Kim, K. Lee, E. Spiecker, P. Schmuki. *Nanoscale.* **2**, 45 (2010).

120. Y. L. Liao, W. X. Que, P. Zhong, J. Zhang, Y. C. He. *ACS Appl. Mater. Interfaces.* **3**, 2800 (2011).

121. Y. L. Liao, X. Y. Wang, Y. B. Ma, J. Li, T. L. Wen, L. J. Jia, Z. Y. Zhong, L. P. Wang, D. N. Zhang. *Cryst Growth Des.* **16**, 1786 (2016).

122. K. Assaker, C. Carteret, B. Lebeau, C. Marichal, L. Vidal, M. J. Stebe, J. L. Blin. *Acs Sustain Chem Eng.* **2**, 120 (2014).

123. Y. L. Liao, J. Brame, W. X. Que, Z. M. Xiu, H. X. Xie, Q. L. Li, M. Fabian, P. J. Alvarez. *J. Hazard. Mater.* **260**, 434 (2013).

124. A. Lamberti, A. Chiodoni, N. Shahzad, S. Bianco, M. Quaglio, C. F. Pirri. *Sci Rep-Uk.* **5**, (2015).

125. B. M. Rao, S. C. Roy. *Rsc Adv.* **4**, 49108 (2014).

126. N. Liu, S. P. Albu, K. Lee, S. So, P. Schmuki. *Electrochim Acta.* **82**, 98 (2012).

127. L. A. Pereira, D. A. D. Almeida, A. B. Couto, N. G. Ferreira. *Mater Res Bull.* **122**, (2020).

128. L. Q. Zhang, H. H. Cao, Y. H. Lu, H. B. Zhang, G. Y. Hou, Y. P. Tang, G. Q. Zheng. *J Solid State Electr.* **24**, 447 (2020).

129. X. Chen, S. S. Mao. *Chem Rev.* **107**, 2891 (2007).

130. K. Nakata, A. Fujishima. *J Photoch Photobio C.* **13**, 169 (2012).

131. S. Riaz, S. J. Park. *J Ind Eng Chem.* **84**, 23 (2020).

132. Y. Liu, J. Li, B. Zhou, X. Li, H. Chen, Q. Chen, Z. Wang, L. Li, J. Wang, W. Cai. *Water Res.* **45**, 3991 (2011).

133. Y. B. Liu, J. H. Li, B. X. Zhou, H. C. Chen, Z. S. Wang, W. M. Cai. *Chem Commun.* **47**, 10314 (2011).

134. V. R. Subramanian, S. Sarker, B. W. Yu, A. Kar, X. D. Sun, S. K. Dey. *J Mater Res.* **28**, 280 (2013).

135. S. P. Albu, A. Ghicov, J. M. Macak, R. Hahn, P. Schmuki. *Nano Lett.* **7**, 1286 (2007).

136. J. Vujancevic, A. Bjelajac, J. Cirkovic, V. Pavlovic, E. Horvath, L. Forro, B. Vlahovic, M. Mitric, D. Janackovic, V. Pavlovic. *Sci Sinter.* **50**, 39 (2018).

137. P. Mazierski, A. Malankowska, M. Kobylanski, M. Diak, M. Kozak, M. J. Winiarski, T. Klimczuk, W. Lisowski, G. Nowaczyk, A. Zaleska-Medynska. *Acs Catal.* **7**, 2753 (2017).

138. S. Nagamine, K. Inohara. *Adv Powder Technol.* **29**, 3100 (2018).

139. S. P. Albu, A. Ghicov, J. M. Macak, P. Schmuki. *physica status solidi (RRL) – Rapid Research Letters.* **1**, R65 (2007).

140. S. Gao, J. Y. Yang, M. Liu, H. Z. Yan, W. X. Li, J. Q. Zhang, Y. B. Luo. *Journal of Power Sources.* **250**, 174 (2014).

141. N. T. Nguyen, I. Hwang, T. Kondo, T. Yanagishita, H. Masuda, P. Schmuki. *Electrochemistry Communications.* **79**, 46 (2017).

142. H. Fraoucene, D. Hatem, F. Vacandio, M. Pasquinelli. *J Electron Mater.* **48**, 2046 (2019).

143. H. Zhou, Y. R. Zhang. *Journal of Power Sources.* **239**, 128 (2013).

144. T. Dikici, M. Yurddaskal, S. Demirci, E. Celik. *J Porous Mat.* **24**, 1535 (2017).

145. Y. K. Lai, L. Sun, Y. C. Chen, H. F. Zhuang, C. J. Lin, J. W. Chin. *J Electrochem Soc.* **153**, D123 (2006).

146. A. J. *Electrochim Acta.* **38**, 43 (1993).

147. J. M. Macak, M. Zlamal, J. Krysa, P. Schmuki. *Small.* **3**, 300 (2007).

148. W. B. Huang, X. Y. Wang, Y. L. Xue, Y. Yang, X. Y. Ao. *Rsc Adv.* **5**, 56098 (2015).

149. X. R. Zhang, Y. H. Lin, D. Q. He, J. F. Zhang, Z. Y. Fan, T. F. Xie. *Chem Phys Lett.* **504**, 71 (2011).

150. D. H. Li, S. W. Lin, S. P. Li, X. Huang, X. K. Cao, J. B. Li. *J Mater Res.* **27**, 1029 (2012).

151. Y. L. Su, X. W. Zhang, S. Han, X. Q. Chen, L. C. Lei. *Electrochemistry Communications.* **9**, 2291 (2007).

152. R. Asahi, T. Morikawa, T. Ohwaki, K. Aoki, Y. Taga. *Science.* **293**, 269 (2001).

153. G. D. Yang, Z. Jiang, H. H. Shi, T. C. Xiao, Z. F. Yan. *J Mater Chem.* **20**, 5301 (2010).

154. X. G. Hou, X. L. Liu, J. Han, H. L. Liu, J. H. Yao, D. J. Li, L. Q. Wang, B. Liao, J. Li, R. J. Zhang. *J Mater Sci.* **55**, 5843 (2020).

155. Y. J. Hwang, S. Yang, H. Lee. *Appl Catal B-Environ.* **204**, 209 (2017).

156. M. Antonopoulou, A. Giannakas, F. Bairamis, M. Papadaki, I. Konstantinou. *Chem. Eng. J.* **318**, 231 (2017).

157. J. H. Park, S. Kim, A. J. Bard. *Nano Lett.* **6**, 24 (2006).

158. C. K. Xu, Y. A. Shaban, W. B. Ingler, S. U. M. Khan. *Sol Energ Mat Sol C.* **91**, 938 (2007).

159. J. Q. Geng, D. Yang, J. H. Zhu, D. M. Chen, Z. Y. Jiang. *Mater Res Bull.* **44**, 146 (2009).

160. S. K. Mohapatra, M. Misra, V. K. Mahajan, K. S. Raja. *Journal of Physical Chemistry C.* **111**, 8677 (2007).

161. C. Di Valentin, G. Pacchioni, A. Selloni. *Chem Mater.* **17**, 6656 (2005).

162. G. Wu, T. Nishikawa, B. Ohtani, A. Chen. *Chem Mater.* **19**, 4530 (2007).

163. S. Karvinen, P. Hirva, T. A. Pakkanen. *J Mol Struc-Theochem.* **626**, 271 (2003).

164. Z. M. El-Bahy, A. A. Ismail, R. M. Mohamed. *J. Hazard. Mater.* **166**, 138 (2009).

165. P. Mazierski, W. Lisowski, T. Grzyb, M. J. Winiarski, T. Klimczuk, A. Mikolajczyk, J. Flisikowski, A. Hirsch, A. Kolakowska, T. Puzyn, A. Zaleska-Medynska, J. Nadolna. *Appl Catal B-Environ.* **205**, 376 (2017).

166. A. Bumajdad, M. Madkour. *Phys Chem Chem Phys.* **16**, 7146 (2014).

167. J. Z. Dong, J. Z. Ye, D. Ariyanti, Y. X. Wang, S. H. Wei, W. Gao. *Chemosphere.* **204**, 193 (2018).

168. X. Fan, J. Wan, E. Z. Liu, L. Sun, Y. Hu, H. Li, X. Y. Hu, J. Fan. *Ceram. Int.* **41**, 5107 (2015).

169. Y. Y. Zhang, H. W. Hu, M. L. Chang, D. C. Chen, M. Zhang, L. P. Wu, X. J. Li. *Ceram. Int.* **43**, 9053 (2017).

170. W. Choi, A. Termin, M. R. Hoffmann. *The Journal of Physical Chemistry.* **98**, 13669 (1994).

171. X. S. Zhou, F. Peng, H. J. Wang, H. Yu, J. A. Yang. *Electrochemistry Communications.* **13**, 121 (2011).

172. L. H. Huang, C. Sun, Y. L. Liu. *Applied Surface Science.* **253**, 7029 (2007).

173. X. Q. Zhang, Y. C. Chai, L. Lin, K. Zhang, B. Zhao, D. N. He. *Catal Lett.* **144**, 987 (2014).

174. Z. B. Dong, D. Y. Ding, T. Li, C. Q. Ning. *Applied Surface Science.* **480**, 219 (2019).

175. H. J. Liu, G. G. Liu, X. Y. Shi. *Colloid Surface A.* **363**, 35 (2010).

176. J. J. Cai, M. H. Zhou, X. Xu, X. D. Du. *J. Hazard. Mater.* **396**, 11 (2020).

177. Z. L. He, W. X. Que, J. Chen, X. T. Yin, Y. C. He, J. B. Ren. *ACS Appl. Mater. Interfaces.* **4**, 6815 (2012).

178. X. Wang, L. L. Wang, D. Guo, L. L. Ma, B. L. Zhu, P. Wang, G. C. Wang, S. M. Zhang, W. P. Huang. *Catal. Today.* **327**, 182 (2019).

179. R. M. Li, G. J. Dong, G. M. Chen. *New J. Chem.* **39**, 6854 (2015).

180. S. In, A. Orlov, R. Berg, F. Garcia, S. Pedrosa-Jimenez, M. S. Tikhov, D. S. Wright, R. M. Lambert. *J Am Chem Soc.* **129**, 13790 (2007).

181. S. Yadav, G. Jaiswar. *J Chin Chem Soc-Taip.* **64**, 103 (2017).

182. S. R. Kim, I. Ali, J. O. Kim. *Applied Surface Science.* **477**, 71 (2019).

183. X. J. Yuan, J. H. Yi, H. J. Wang, H. Yu, S. Q. Zhang, F. Peng. *Mater Chem Phys.* **196**, 237 (2017).

184. W. Teng, Y. M. Wang, H. H. Huang, X. Y. Li, Y. B. Tang. *Applied Surface Science.* **425**, 507 (2017).

185. L. Yang, X. Bai, J. Shi, X. Y. Du, L. Xu, P. K. Jin. *Appl Catal B-Environ.* **256**, (2019).

186. S. R. Mirmasoomi, M. M. Ghazi, M. Galedari. *Sep Purif Technol.* **175**, 418 (2017).

187. D. W. Gao, L. Wang, Q. Y. Wang, Z. M. Qi, Y. Jia, C. X. Wang. *Spectrochim Acta A.* **229**, (2020).

188. X. Q. Kong, J. Y. Li, C. W. Yang, Q. Tang, D. Wang. *Sep Purif Technol.* **248**, (2020).

189. E. Mugunthan, M. B. Saidutta, P. E. Jagadeeshbabu. *Environmental Nanotechnology, Monitoring and Management.* **10**, 322 (2018).

190. L. M. Sun, X. X. He, Y. S. Yuan, J. Q. Chen, W. W. Zhan, X. J. Wang, Y. L. Zhao, X. G. Han. *Chem. Eng. J.* **397**, 11 (2020).

191. K. Perovic, F. M. dela Rosa, M. Kovacic, H. Kusic, U. L. Stangar, F. Fresno, D. D. Dionysiou, A. L. Bozic. *Materials.* **13**, 44 (2020).

192. M. H. Sun, X. G. Wang, Z. Q. Chen, M. Murugananthan, Y. Chen, Y. R. Zhang. *Appl Catal B-Environ.* **273**, 13 (2020).

193. R. Macias-Tamez, M. Villanueva-Rodriguez, N. A. Ramos-Delgado, L. Maya-Trevino, A. Hernandez-Ramirez. *Water Air Soil Pollut.* **228**, 12 (2017).

194. A. Kaur, D. B. Salunke, A. Umar, S. K. Mehta, A. S. K. Sinha, S. K. Kansal. *New J. Chem.* **41**, 12079 (2017).

195. K. Z. Qi, B. Cheng, J. G. Yu, W. K. Ho. *Chinese J Catal.* **38**, 1936 (2017).

196. L. J. Zhang, S. Li, B. K. Liu, D. Wang, T. F. Xie. *Acs Catal.* **4**, 3724 (2014).

197. J. J. Xian, D. Z. Li, J. Chen, X. F. Li, M. He, Y. Shao, L. H. Yu, J. L. Fang. *ACS Appl. Mater. Interfaces.* **6**, 13157 (2014).

198. X. T. Zheng, L. M. Yang, Y. B. Li, L. X. Yang, S. L. Luo. *Electrochim Acta.* **298**, 663 (2019).

199. Z. P. Yan, W. C. Wang, L. L. Du, J. X. Zhu, D. L. Phillips, J. S. Xu. *Appl Catal B-Environ.* **275**, 10 (2020).